NUREG/CR-3379
SAND83-7114
R7
Printed December 1983
CONTRACTOR REPORT

SLAM - A Sodium-Limestone Concrete Ablation Model

A. J. Suo-Anttila
Sandia National Laboratories
Albuquerque, NM 87185

Prepared by
Sandia National Laboratories
Albuquerque, New Mexico 87185 and Livermore, California 94550
for the United States Department of Energy
under Contract DE-AC04-76DP00789

Prepared for
U. S. NUCLEAR REGULATORY COMMISSION

Available from
GPO Sales Program
Division of Technical Information and Document Control
U.S. Nuclear Regulatory Commission
Washington, D.C. 20555

and

National Technical Information Service
Springfield, Virginia 22161

NUREG/CR-3379
SAND83-7114
R7

SLAM - A SODIUM-LIMESTONE CONCRETE ABLATION MODEL

A. J. Suo-Anttila

Printed: December 1983

Sandia National Laboratories
Albuquerque, New Mexico 87185
Operated by
Sandia Corporation
for the
U.S. Department of Energy

Prepared for
Division of Reactor Safety Research
Office of Nuclear Regulatory Research
U.S. Nuclear Regulatory Commission
Washington, DC 20555
Under Memorandum of Understanding DOE 40-550-75
NRC FIN No. A1054

Abstract

The Sodium Limestone Ablation Model (SLAM) is described in detail in this report. SLAM is a three-region model, containing a pool (sodium and reaction debris) region, a dry (boundary layer and dehydrated concrete) region, and a wet (hydrated concrete) region. The model includes a solution to the mass, momentum, and energy equations in each region. A chemical kinetics model is included to provide heat sources due to chemical reactions between the sodium and the concrete.

Both isolated model as well as integrated "whole code" evaluations have been made with good results. The chemical kinetics and water migration models were evaluated separately, both with good results. Several small and large-scale sodium limestone concrete experiments were simulated with reasonable agreement between SLAM and the experimental results.

The SLAM code was applied to investigate the effects of mixing, pool temperature, pool depth and fluidization. All these phenomena were found to be of significance in the predicted response of the sodium concrete interaction. Pool fluidization is predicted to be the most important variable in large scale interactions.

Table of Contents

List of Figures

Sodium-Limestone-Ablation-Model

1. Introduction

Liquid Metal Fast Breeder Reactors (LMFBR's) utilize large quantities of liquid sodium as the coolant. Because liquid sodium is highly chemically reactive, safety issues concerning the possible contact between the coolant and the concrete used in the reactor containment building, are being addressed. Vigorous chemical reactions have been observed between liquid sodium and concrete in a number of experiments.[1-4] These chemical interactions ultimately result in concrete ablation, heat and hydrogen generation, and aerosol production. All of these phenomena must be considered when evaluating containment safety margins, especially if the chemical interaction is rapid and extensive.

2. Sodium-Concrete Interaction Experiments

A large number of experiments concerning the interaction of sodium and concrete have been conducted. Variables in these experiments include concrete type, sodium depth and temperature, external heat sources, and experiment size (scaling effects).

Concrete type is an important parameter, because it determines the nature of the chemical reactions that occur. Typically the structural concrete used in a reactor will consist of portland cement mixed with local sand and gravel. The chemical composition of the sand and gravel (aggregate) will depend upon the geographical location of the quarry and therefore is expected to vary considerably from one reactor to the next. Fortunately from the available experimental evidence it appears that there are only two main types of interactions that will occur, unless the concrete is of a special type. The two main interactions that have been seen are those between sodium and silicates and those between sodium and carbonate containing materials. The rate and extent of interaction depends upon the type of concrete; i.e., siliceous or carbonaceous.[1-4]

Experimentally observed sodium concrete interactions often display a well defined behavior pattern provided the experiment is conducted at a high enough temperature.[1] Initially when hot sodium contacts concrete, the high temperatures cause water to evaporate from the concrete. The evolving steam reacts with the liquid sodium to produce sodium hydroxide and hydrogen gas. This activity persists for some time and has been termed Phase 1 by SNLA investigators.[2] If the aggregate is of a reactive type, then a transition to Phase 2 often occurs. Phase 2 of sodium-concrete

interactions is characterized by concrete ablation, sodium-aggregate reactions and hydrogen, aerosol and heat production, all at rates of about an order of magnitude greater than those found in Phase 1. Typical ablation rates are on the order of 1 mm/min., with variations as large as a factor of four. Ablation (or penetration) refers to the rate at which the concrete is chemically and physically degraded. The degradation occurs in a planar mode, where the reaction plane moves into the concrete at the ablation velocity (or penetration rate).

Sodium depth and temperature have been found to have some effect upon limestone concrete interactions. The transition from the mild phase to the energetic phase seemed to correlate with pool depth in some early SNLA limestone experiments(P1-P3).[3] However the correlation could not be extended to later tests that were conducted in a different manner (i.e. inert atmospheres, pool heaters, and different sodium pour temperatures). This seems to indicate that many parameters are involved in addition to pool depth. Many small-scale experiments have indicated a threshold temperature around 550°C below which energetic limestone reactions will not occur and above which they will occur.[5,6] The existence of a threshold temperature is not as well established for silicate concretes. Indeed an experiment conducted in Germany became energetic at a sodium temperature as low as 250°C.[7] The concrete in this case was a very high silica type (quartz aggregate) reacting in an open air environment.

Scale is apparently an important variable, since several large-scale experiments have behaved differently than small-scale experiments. The rate and extent of penetration (ablation) has often been found to be greater in large-scale (~1m dia) compared to small-scale (~1/3m dia) experiments in short-term tests (less than 4 hours).

3. Sodium-Concrete-Models

The results of the experiments lead to confusing and sometimes conflicting results. Even when an experiment is repeated exactly as possible, the result is only approximately reproducible. Thus, the nature of sodium-concrete interaction seems to depend upon many parameters some of which are so subtle that investigators may overlook them altogether. The best way to correlate the existing experimental data and to understand the nature of the many parameters involved is to develop a self-consistent model.

A sodium concrete interaction model, when completed, should provide a detailed mechanistic understanding of the most relevant phenomena. It should be flexible enough so that different theories concerning the details of the interaction can be

included, and therefore quantitatively evaluated. A quantitative comparison with experiment allows the analyst to discard phenomena that are irrelavent to the model, and more importantly, it will act as a guide in selecting phenomena that are very important. Finally, if the model is quantitatively correct, then it can be used as a predictive tool in guiding future research in the area, and in making LMFBR safety evaluations.

Presently to the authors knowledge there are three modeling efforts for sodium concrete interactions: Hanford Engineering Development Laboratories (HEDL)[8], the French[9], and Sandia National Laboratories (SNLA) all have ongoing analytical efforts in developing sodium concrete interaction models. The purpose of this paper is to describe the current SNLA model for sodium-limestone concrete interactions, and to present some preliminary model evaluations and applications.

The current modeling effort at SNLA is an extension of the now completed Sodium Concrete Ablation Model (SCAM)[10] development project. The SCAM model was developed by the author to model sodium attacking basaltic concrete in a steady state mode. The main features of the SCAM model are that the sodium is transported to the reaction zone in the vapor phase. The rate of energy production by chemical reaction is balanced by the energy required to heat the concrete and evaporate the sodium. Thus the penetration rate is governed by a complex combination of sodium vapor transport and chemical kinetics. Since the sodium vapor transport is affected by pressure, the model predicts a penetration rate that is dependent upon the system pressure. This seems to explain some of the differences between some SNLA[2] and HEDL[1] large-scale experiments with basaltic concrete because they were conducted at significantly different altitudes, and also between some HEDL large-scale (at ambient pressure) and small-scale experiments which were conducted in a self-pressurizing apparatus. To date a systematic experimental effort to quantify the predicted pressure effect has not been initiated because silica concretes are currently a lower priority than carbonate concretes.

The SNLA model for limestone concrete interactions described herein is called Sodium-Limestone-Ablation Model (SLAM). SLAM in its current formulation does not consider vapor phase transport of sodium, instead the major resistance to sodium transport is by turbulent diffusion within a liquid slurry. Vapor phase transport of sodium would be important in SLAM if the mass transfer resistance of vapor phase transport were of the same order or greater than slurry diffusional resistances. If vapor phase transport is in fact important then one would expect a similar dependence upon the pressure as is predicted by SCAM, thus there is an experimental way of determining whether or not

vapor phase activity is important. Lastly if pressure effects are found to be significant experimentally then the SLAM would need to be modified by adding a vapor diffusion resistance in series with the slurry diffusional resistance.

4. Sodium Limestone Ablation Model (SLAM) Description

SLAM was chosen to be a fully transient model in order to account for the transition from phase 1 to phase 2, reactant depletion, and reaction product accumulation effects. By modeling all of these effects direct comparisons with existing experimental data can be made.

In the Transient SLAM code there exist three distinct regions as depicted in Figure 1. The pool region, as the name implies, contains the sodium pool and all of the reaction products from the sodium-concrete reaction. It can also contain unreacted concrete. The purpose of the pool region is to supply a thermal and composition boundary conditions for the dry region directly below it. The temperature of the pool region is assumed to be uniform and so its time behavior is calculated by a bulk energy equation. The pool composition is tracked in time by a set of continuity equations that describe the distribution of each important chemical species. Chemical reactions with their accompanying heat production are allowed to occur in the pool region. The same rate equations that are used in the reaction zone are also used in the pool region.

The dry region contains the dehydrated concrete region and the boundary layer of the pool region. The boundary layer is included in the dry region so that a fine resolution of the temperature and composition profiles can be achieved without defining a separate (4th) region. The size of the dry region is calculated by integrating the effects of growth due to evaporation and migration of liquid water at the wet region boundary, and shrinkage due to ablation of the dehydrated concrete. The size of the boundary layer is chosen by the user as some fraction of the dry zone and will be discussed further in section 7.3.

At the interface between the dehydrated concrete and the pool boundary layer, ablation is presumed to occur by one of two mechanisms. The first is dissolution; that is, the concrete is assumed to dissolve to its saturation point in the liquid material of the boundary layer and is then transported away by turbulent diffusion. Since the dissolved concrete constituents are chemically reactive with the sodium in the boundary layer greatly enhanced penetration rates will occur due to steepening

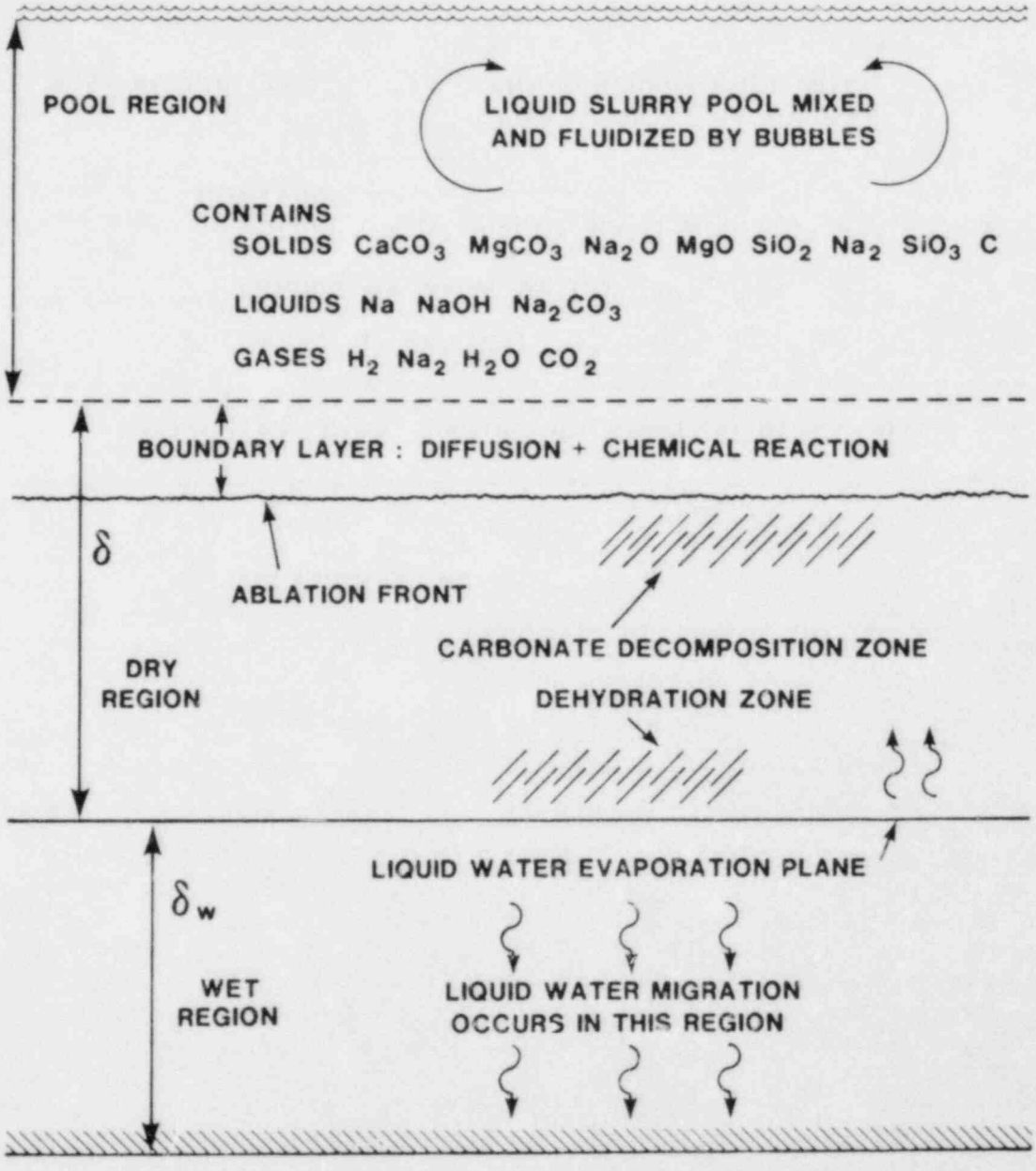

Figure 1. Schematic diagram of the sodium limestone ablation model.

of the concentration gradients caused by chemical reaction with sodium. The second mechanism of concrete ablation is chemical reaction. If sodium is present at the concrete interface, a chemical reaction is assumed to occur with the concrete. The reaction products are of a liquid slurry nature and by definition now belong to the pool region. Thus, ablation has occurred. The ablation rate in this case depends upon the kinetics of the chemical reaction between sodium and the concrete constituents.

Some of the heat generated within the boundary layer is conducted into the dehydrated concrete which releases the chemically bound H_2O and CO_2 gases. This degassing phenomena is accompanied by the absorbtion of heat energy. Thus in the dry region there are both volumetric heat sources due to chemical reaction within the boundary layer and heat sinks due to gas generation in the dehydrated concrete.

In the dry region there are three basic equations that are solved; a set of continuity equations that describe the composition distributions, an energy equation that describes the temperature distribution, and a momentum equation that describes the pressure distribution. The pressure distribution is not important in itself, with the exception of the pressure at the dry zone - wet zone interface. Since liquid water exists at this interface and thermodynamic equilibrium between phases is assumed to prevail the pressure is tied directly to the temperature at this interface. The interface pressure also provides a driving force for liquid water migration in the wet zone.

The wet zone is that region of concrete that contains liquid water. The distribution of liquid water is important because it determines the amount which can be evaporated. The evaporated water is then available for chemical reaction in the boundary layer. The liquid water can move through the pores of the concrete under the influence of a pressure gradient. It can also evaporate at the wet-dry interface thereby leaving the wet zone. There are three types of equations that are solved in this region: continuity, momentum and energy. The continuity equations in this region are those for liquid water and air. The distribution of air in the wet zone combined with the liquid water and porosity distribution determines the pressure distribution. Two momentum equations (Darcy's Law) are solved based upon the pressure distribution. The momentum equations determine the relative motions of the water and air within the wet zone.

5. Coordinate Systems

In SLAM there exist three distinct regions; the pool, the dry zone, and the wet zone. As time passes and penetration occurs, each region will change its size and position. There are two classical coordinate systems with which one can describe distributions within a region, Eulerian and Lagrangian. The Eulerian system is typically fixed in space with material flowing through it. The Lagrangian system is usually attached to the material that is flowing and moves with it. In the SLAM model the material remains fixed but the boundaries of each region change position with time. A fixed Eulerian system is a poor choice, because nodes must be added or subtracted as the boundaries move. This causes jumping and jolting of the distributions within the boundaries, which can be especially severe if the most important phenomena are close to a boundary, such as in the boundary layer region. A Lagrangian system does not apply because the material is fixed in space.

A moving Eulerian system turns out to be a good choice for concrete ablation problems. In this case the coordinate system is attached to the boundaries of the region or to some significant point within the region and moves with it according to the physics of the problem. This choice of coordinate system reduces many of the numerical diffusion and mass loss problems encountered in multi-component problems because distributions tend to become stationary within the coordinate system as motion occurs. The transformation from fixed to moving coordinates amounts to adding an advective term with the material velocity equal to the negative of the coordinate system velocity.

Figure 2 shows the coordinate systems used in SLAM.

In the pool region the material is assumed to be well mixed and virtually isothermal. During penetration the pool changes in composition which results in swelling with time. The swelling is caused by the addition of gases and reaction products of lower density than the reactants. The coordinate system within the pool is fixed to its boundaries, and the nodes within are of variable size according to their fixed number and the amount of swelling that has occurred.

Almost all of the important activity occurs within the boundary layer of the dry region. This region can swell or shrink, and it moves with the penetration front. These various motions can be quite rapid, especially at early times, so they must be completely embodied within the equations that are solved. The coordinate system in this region is attached to the interface between the concrete and the liquid boundary layer. This

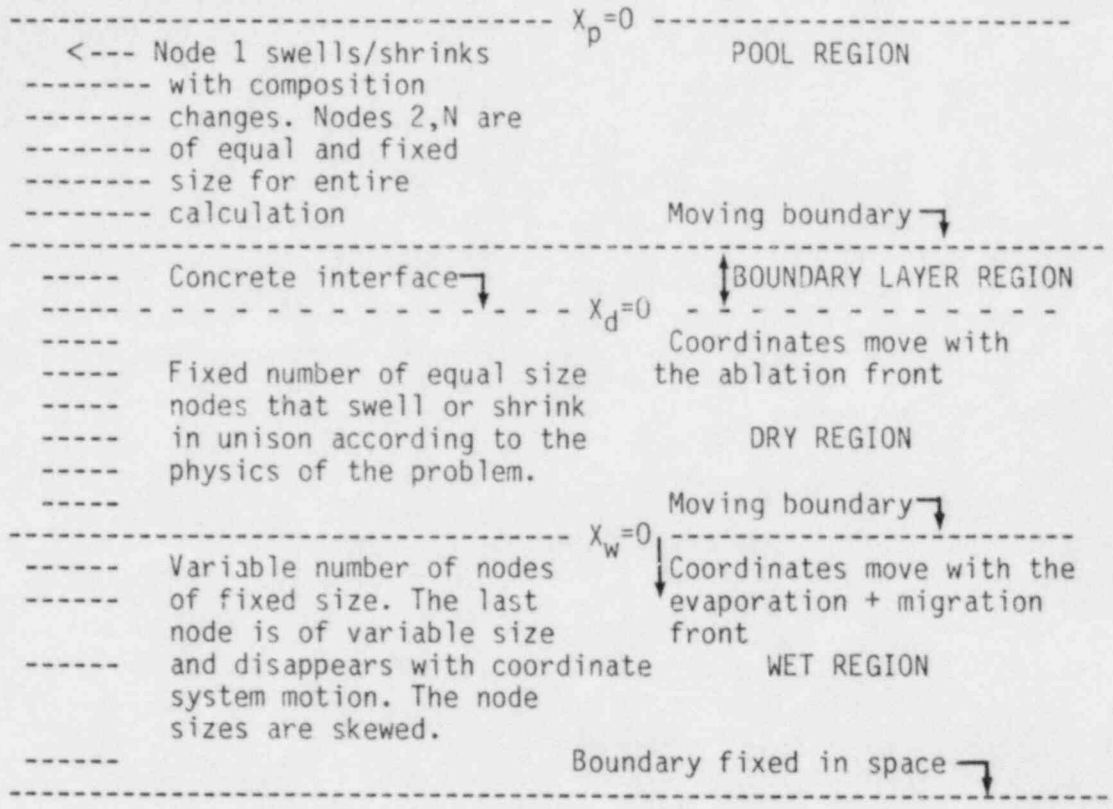

Figure 2. The SLAM Coordinate Systems
Subscripts p, d, and w refer to pool, dry, and wet respectively

location was chosen because the coordinate system velocity is the penetration rate regardless of the degree of swelling or shrinkage that takes place.

The wet zone is somewhat unique in concrete ablation problems because its behavior is always the same, that is, it dries up and disappears. Because its behavior is always the same, though the rates may differ from problem to problem, certain advantages can be taken to improve the accuracy and speed of calculation. The coordinate system is attached to the liquid water evaporation plane. Since this is the hottest location in the wet zone, a skewed coordinate system is utilized. The node size distribution is chosen by an inverse power law applied to a given thickness of concrete and a given number of nodes. A typical problem results in nodes that are a few millimeters next to the origin, growing to fractions of a meter at the other

boundary. The skewed node size was chosen so that temperature gradients at the origin could be resolved to a high degree of accuracy. Temperature resolution at the origin is important in determining the motion of the boundary as well as the migration of liquid water. At the cold (opposite) boundary virtually nothing happens, therefore the last node is allowed to shrink and disappear from the calculation as motion of the coordinate system occurs. Note that node sizes do not change in this region, with the exception of the last node.

6. Solution of Conservation Equations

The SLAM code consists of a simultaneous solution in time of a large number of conservation equations that describe the most important aspects of sodium-concrete ablation. The conservation equations are of three main types; continuity, momentum and energy. The conservation equations are solved in each of the three regions. There is one continuity equation for each of the 15 possible chemical species, and an overall continuity equation for total mass conservation. Thus since there are three regions one might expect (15 + 3) x 3 = 54 simultaneous partial differential equations. However, some of these equations can be deleted from the set. For example, most of the chemical species do not exist in the wet zone so they can be deleted. The pressure distribution in the pool region is irrelevant unless sodium vaporization is considered. Thus the final tally of relevant conservation equations are: 17 pool (15 species, 1 overall continuity, 1 energy): 18 dry region (15 species, 1 overall continuity, 1 momentum, 1 energy): and 5 wet region (2 continuity, 2 momentum, 1 energy): or 40 conservation equations in all. Of these equations, all but two are solved using finite-difference techniques. The two equations that are not solved by finite difference are: the momentum equation in the dry region which is solved by numerical integration and the energy equation in the dry region which is solved by the Galerkin method.

6.1 The Continuity Equations

There are currently 16 continuity equations, one for each species and one overall continuity equation to insure conservation of total mass. The 15 chemical species that are treated are SiO_2, H_2O, Na, H_2, NaOH, Na_2SiO_3, Na_2CO_3, Na_2O, CaO, $CaCO_3$, CO_2, C, $MgCO_3$, MgO and inert material. The inert material is the sum of all other chemicals that have a significant mass but negligible chemical reaction. The general continuity equation for each chemical species is:

$$\frac{\partial \rho i}{\partial t} + \frac{\partial \rho i}{\partial x}\frac{dx}{dt} + V\frac{\partial \rho i}{\partial x} = \frac{\partial}{\partial x}\gamma\frac{\partial \rho i}{\partial x} + \sum S_i$$

Summing these equations results in an overall mass conservation equation

$$\text{Div } V = \sum \frac{Si}{Di}$$

which simply states that the divergence of the material velocity (V) is equal to the rate of volume generation due to chemical reaction or other sources and sinks.

The macroscopic density of material i (ρi) is defined as the mass of material i in a unit volume, whereas the microscopic density Di refers to the density of pure material. In both cases the units are Kg/m^3. The five terms which appear in the general continuity equation are:

$\frac{\partial \rho i}{\partial t}$ is the net rate of change of macroscopic density of species i

$\frac{\partial \rho i}{\partial x}\frac{dx}{dt}$ is the rate of change due to coordinate system swelling or shrinkage

$V\frac{\partial \rho i}{\partial x}$ is the rate of change due to coordinate system motion

$\frac{\partial}{\partial x}\gamma\frac{\partial \rho i}{\partial x}$ is the rate of change due to turbulent diffusion, where γ is the mass exchange coefficient

$\sum S_i$ is the sum over sources and sinks due to chemical reaction

The continuity equations are solved using a three-step procedure to improve numerical stability. The steps are solved sequentially with the intermediate density appearing as the beginning of time step density in the next step. By summing the finite-differenced steps the original equation is obtained. The error that is introduced by this scheme comes from using intermediate time step densities to describe the various processes. The magnitude of the error can be made small if small time steps are used, even though the procedure is stable for any time step size.

Step 1: calculate the change due to sources/sinks

$$\frac{\partial \rho i}{\partial t} = \sum S_i$$

The sources and sinks are due to chemical reaction, gas generation or motion across a region boundary. In solving the continuity equations no flow boundary conditions are used, and hence material that crosses a region boundary is treated as a source or sink depending upon the direction of flow. For material that crosses a region boundary the mass source/sink term is

$S_i = V_B \rho_{id}$ where V_B is the material velocity crossing the boundary and ρ_{id} is the density of material i in the donor cell. A donor cell is defined as the finite difference node that donates material i.

This step is solved by implicit finite-difference (see sec 7.1)

Step 2.

Diffuse the intermediate end of time step density from step 1.

$$\frac{\partial \rho i}{\partial t} = \frac{\partial}{\partial x} \gamma \frac{\partial \rho i}{\partial x}$$

This step is solved by a fully-implicit finite-difference method. A forward-elimination backward-substitution algorithm is employed.

Step 3.

Solve simultaneously the species advection and the overall continuity equation.

a) The species advection equation is

$$\frac{\partial \rho i}{\partial t} + V\frac{\partial \rho i}{\partial x} + \frac{\partial \rho i}{\partial x}\frac{dx}{dt} = 0$$

where $\frac{dx}{dt}$ is the local rate of coordinate system growth. In solving the finite-difference form of the continuity equation, the growth term is included in the definition of the velocities of the cell boundaries. Physically, the growth term accounts for material that appears in the coordinate system because of a change in the extent of the coordinate system.

In semi implicit finite difference form the advection equation is

$$\rho_j^{n+1} = \frac{\frac{\rho_j^n}{\Delta t} + \frac{\rho_{j-1}^n V_j^+ - \rho_{j+1}^{n+1} V_{j+1}^-}{\Delta x}}{\frac{1}{\Delta t} + \frac{(V_{j+1}^+ - V_j^-)}{\Delta x} + \dot{\delta}/\delta}$$

where j is the finite difference node and the velocities are defined according to a donor cell formulation with a swelling/shrinking coordinate system.

$$V_j^+ = \max\left(0 , V(j) - \dot{\delta}\, x(j) \right)$$

$$V_j^- = \min\left(0 , V(j) - \dot{\delta}\, x(j) \right)$$

$$V^{+}_{j+1} = \max\left(0 , V(j+1) - \dot{\delta}\, x(j+1) \right)$$

$$V^{-}_{j+1} = \min\left(0 , V(j+1) - \dot{\delta}\, x(j+1) \right)$$

δ is the region thickness and the dot implies time derivative

Note that in the above equation the material subscript i has been deleted so that the node subscript j can be shown more explicitly.

The $\dot{\delta}$ term is set to zero in the pool and wet regions because it is negligible in comparison to the other terms. In the dry region it is quite significant especially at early times when growth rates are large.

Step 3b. Solve the overall mass continuity equation. The simplest method is to select a velocity V(x) such that mass is conserved. For each node j, the velocity at the j + 1 interface is calculated such that

$$\sum \frac{\rho_i^{n+1}}{D_i} = 1$$

in other words a velocity at the j + 1 interface is found such that the sum of the volume fractions of all the components within a node equals 1. This is equivalent to conserving mass because the materials are treated as fully incompressible and therefore the volume fractions are directly related to the macroscopic densities through the microscopic densities. Numerically the velocity is found using a Newton-Raphson technique. A function is defined

$$F = 1 - \sum \frac{\rho_i^{n+1}}{D_i}$$

which is differentiated numerically by iteration k and a new velocity is calculated

$$V_{j+1}^{k+1} = V_{j+1}^{k} - F/\frac{dF}{dV}$$

Steps 3a and b are repeated at each node j until F is suitably small; ~0.0001. Although Step 3 insures overall continuity of mass, it does not prevent mass loss due to numerical diffusion,or error accumulation. Mass loss due to numerical diffusion is well known in multicomponent problems and can best be avoided by the use of small nodes and short time steps if finite-difference methods are employed. Error accumulation occurs because F is not reduced to zero; hence, a small mass error is created each time step. Error accumulation can be minimized by running problems that do not exceed a couple of thousand time steps or by reducing the error criterion on F even further. Note that smaller values of F requires greater numerical precision which is computing machine dependent. In all of the simulations that appear in this report a VAX 11-780 computer was used in the single precision mode giving 7 digits of accuracy.

6.2 The Energy Equations

There are three energy equations in SLAM and each one is solved in a different manner. In the pool region a bulk energy equation appears because it is assumed that good mixing occurs in this region and hence the temperature is uniform. In the dry zone the Galerkin method is used to solve the energy equation because it minimizes numerical diffusion. In the wet zone a semi-implicit difference method is used to solve the energy equation.

6.2.1 The Pool Region:

The bulk temperature of the pool, T_p, can be determined by summing the energy sources and sinks. The resulting equation is

$$\rho\, c\, \delta_p \frac{\partial T_p}{\partial t} = q_o + h_\infty (T_\infty - T_p) + \varepsilon\sigma (T_\infty^4 - T_p^4) - \Delta\dot{m}\, h_{fg} + Q + Pw$$

where

ρ = average pool density (Kg/m^3)

c = average pool specific heat (J/Kg-K)

δ_p = pool depth (m)

q_o = the heat flux at the top of the dry region (W/m^2)

h_∞ = a convective heat transfer coefficient at the top of the pool

ε = radiant emissivity of the pool surface

σ = Stefan Boltzman constant (5.76×10^{-8} W/m^2K^4)

T_∞ = ambient temperature above the pool surface (K)

$\Delta\dot{m}$ = the evaporative mass flux of sodium (Kg/m^2-sec)

Q = the heat generation due to chemical reaction (W/m^2)

Pw = the external heater power level (W/m^2)

h_{fg} = the latent heat of sodium vaporization (J/Kg)

The evaporative mass flux of sodium is the additional evaporation of sodium vapor that occurs in the pool. At the bottom boundary of the pool region, hydrogen gas saturated with sodium vapor enters. The H_2 comes from reactions that take place within the boundary layer region. Since hydrogen forming reactions can occur within the pool region, there will be additional sodium evaporation to maintain the gases that leave in a saturated state. If P_∞ is the pressure in the pool region and P_s is the saturation pressure of sodium vapor, then the additional mass flux of sodium vapor from the pool is

$$\Delta\dot{m} = \frac{\Delta\dot{m}_{H_2}}{W_{H2}} \frac{Ps}{P_\infty - Ps} W_{Na}$$

where $\Delta\dot{m}_{H2}$ is the net mass flux of H_2 gas generated within the pool region by chemical reaction, and W is the molecular weight.

The pool thermal energy equation is finite differenced in time, and solved implicitly by iteration. Iteration is required because sodium evaporation, chemical reaction heat sources, and

the thermal radiation are nonlinear functions of pool temperature.

6.2.2 The Dry Region

The energy equation in the dry region is subject to a large number of variations. The region moves, changes size, has both heat sources and sinks, time dependent boundary conditions, and variable properties due to chemical reactions. All of these phenomena will have a significant influence upon the final solution so they must be fully accounted for in the solution technique.

The energy equation in the dry region is

$$\frac{\partial T}{\partial t} + V\frac{\partial T}{\partial x} = \frac{1}{\rho c}\frac{\partial}{\partial x}K\frac{\partial T}{\partial x} + \frac{Q_v}{\rho c}$$

where T is the temperature (K)

V is the negative coordinate system velocity (m/sec)

ρ is the material density (Kg/m^3)

c is the material specific heat (J/Kg-K)

K is the thermal conductivity (W/m-K)

Q_v is the volumetric heat source or sink (W/m^3)

The boundary conditions are

at $x = 0$ $T = T_p = T_{pool}$

at $x = \delta(t)$ $T = T_s$

At $\delta(t)$, which is the dry zone - wet zone interface location, the temperature (T_s) is the saturation temperature of water because this is where the liquid water evaporates. T_s is not the boiling point because the evaporated water must first pass thru a frictional material before reaching the reaction zone which is at the sum of atmospheric pressure plus the pool head.

The Galerkin method is used to solve the energy equation in the dry region since it can be applied without any loss of generality or accuracy in spite of the many variations that are

taking place. In utilizing the Galerkin method the temperature is approximated by a series representation that satisfies the boundary conditions. The series chosen for the dry region is

$$T(x,t) = T_p + (T_s - T_p)\frac{x}{\delta} + \sum_{m=1}^{N} A_m(t) \sin\frac{m\pi x}{\delta}$$

Where N is a user chosen number of terms - typically 6 to 12 depending upon the solution accuracy desired, and δ is the thickness of the dry zone.

Substituting this series into the energy equation results in:

$$\dot{T}_p + (\dot{T}_s - \dot{T}_p)\frac{x}{\delta} - (T_s - T_p)\frac{x}{\delta^2}\dot{\delta} + \sum_{m=1}^{N}\left[\dot{A}_m \sin(\frac{m\pi x}{\delta})\right.$$

$$\left. - A_m\left(\frac{m\pi x\dot{\delta}}{\delta^2} + V\frac{m\pi}{\delta}\right)\cos(\frac{m\pi x}{\delta})\right] =$$

$$\frac{1}{\rho c}\frac{dK}{dx}\left[\frac{Ts - Tp}{\delta} + \sum_{m=1}^{N} A_m \frac{m\pi}{\delta}\cos(\frac{m\pi x}{\delta})\right]$$

$$- \frac{K}{\rho c}\sum_{m=1}^{N} A_m\left(\frac{m^2\pi^2}{\delta^2}\right)\sin\left(\frac{m\pi x}{\delta}\right) + \frac{Qv}{\rho c}$$

The dots above the symbols imply time derivative. Note that time derivatives of the boundary temperatures $\dot{T}_s$ and $\dot{T}_p$ as well as the region size $\dot{\delta}$ appear naturally from the differentiation.

In order to solve for the unknown coefficients $A_m(t)$ the equation is weighted by

$$\sin(\frac{n\pi x}{\delta})dx$$

and integrated over the region dimensions. The result is N simultaneous ordinary differential equations for the unknown coefficients $A_m(t)$. The equations are

$$\dot{A}_m \frac{\delta_{mn}}{2} + A_m \left[-\frac{m\pi\dot{\delta}}{\delta^2} I_1 + \frac{Vm\pi}{\delta} I_2 - \frac{m\pi}{\rho c \delta} I_3 + \frac{m^2\pi^2}{\rho c \delta^2} I_4 \right]$$

$$= \dot{T}_p I_5 - \left[\frac{(\dot{T}_s - \dot{T}_p)}{\delta} - \right.$$

$$\left. (T_s - T_p) \frac{\dot{\delta}}{\delta^2} + \frac{(T_s - T_p)}{\rho c \delta} \right] I_6 + \frac{I_7}{\rho c}$$

where the I's are the following integrals

$$I_1 = \int_0^\delta x \cos\left[\frac{m\pi x}{\delta}\right] \sin\left[\frac{n\pi x}{\delta}\right] dx$$

$$I_2 = \int_0^\delta \cos\left[\frac{m\pi x}{\delta}\right] \sin\left[\frac{n\pi x}{\delta}\right] dx$$

$$I_3 = \int_0^\delta \frac{dK}{dx} \cos\left[\frac{m\pi x}{\delta}\right] \sin\left[\frac{n\pi x}{\delta}\right] dx$$

$$I_4 = \int_0^\delta K \sin\left[\frac{m\pi x}{\delta}\right] \sin\left[\frac{n\pi x}{\delta}\right] dx$$

$$I_5 = \int_0^\delta \sin\left[\frac{n\pi x}{\delta}\right] dx$$

$$I_6 = \int_0^\delta x \sin\left[\frac{n\pi x}{\delta}\right] dx$$

$$I_7 = \int_0^{\delta} Qv \sin\left[\frac{n\pi x}{\delta}\right] dx$$

All or the integrals except 3, 4 and 7 can be evaluated analytically. In order to improve the speed of the numerical integrations of I_3 and I_4 the thermal conductivity can be redefined as

$$K = K'(x) + \bar{K}$$

where K' is a position dependent thermal conductivity and $\bar{K}$ is a constant average thermal conductivity. Utilizing this definition of thermal conductivity the integrals become

$$I_3 = \int_0^{x'} \frac{dK'}{dx} \cos\left[\frac{m\pi x}{\delta}\right] \sin\left[\frac{n\pi x}{\delta}\right] dx$$

$$I_4 = \bar{K} \frac{\delta_{mn}}{2} + \int_0^{x'} K' \sin\left[\frac{m\pi x}{\delta}\right] \sin\left[\frac{n\pi x}{\delta}\right] dx$$

These integrals are quicker to evaluate numerically because the limits of integration are only over the range where variations in thermal conductivity occur (from 0 to x'). In the dry region this corresponds to the reaction zone (boundary layer). Large variations in thermal conductivity occur in the reaction zone because it consists of entirely different material than the concrete, and ongoing chemical reactions are continuously changing the composition. In the concrete part of the dry zone, the thermal conductivity is assumed spatially constant, though it is allowed to vary in time with the average temperature of this region.

The simultaneous set of ordinary differential equations for the unknown coefficients $A_m(t)$ are solved by implicit finite differencing and subsequent matrix inversion. The matrix equation for the end of time step coefficient (A_m^{n+1}) is:

$$A_m^{n+1}\left[\frac{\delta_{mn}}{2} - \frac{m\pi\dot{\delta}}{\delta^2} I_1 + \frac{Vm\pi}{\delta} I_2 - \frac{m\pi}{\rho c\delta} I_3 + \frac{m^2\pi^2}{\rho c\delta^2} I_4\right]$$

$$= \Delta t\left[-\dot{T}_p I_5 - \left[\frac{(\dot{T}_s-\dot{T}_p)}{\delta} - (T_s-T_p)\frac{\dot{\delta}}{\delta^2} + \frac{(T_s-T_p)}{\rho c\delta}\right] I_6 + \frac{I_7}{\rho c}\right]$$

$$+ A_m^n \frac{\delta_{mn}}{2}$$

Note that in this equation superscript n refers to time step, whereas subscript n refers to the n'th equation.

After the end of time step coefficients A_m^{n+1} are solved for, the heat flux at the boundaries as well as the temperature distribution can be evaluated. The heat flux at the boundaries is

$$q_0 = -K\left.\frac{\partial T}{\partial x}\right|_{x=0} = -K\left[\frac{(T_s-T_p)}{\delta} + \sum Am\,\frac{m\pi}{\delta}\right]$$

$$q_\delta = -K\left.\frac{\partial T}{\partial x}\right|_{x=\delta} = -K\left[\frac{(T_s-T_p)}{\delta} + \sum Am\,\frac{m\pi}{\delta}\cos(m\pi)\right]$$

The temperature distribution can be evaluated at any location from its definition.

6.2.3 The Wet Region

The energy equation in the wet zone is the same as that in the dry zone except that there are no heat sources, i.e.,

$$\frac{\partial T}{\partial t} + Vw \frac{\partial T}{\partial x_w} = K \frac{\partial^2 T}{\partial x_w^2}$$

where Vw is the negative of the wet zone coordinate system velocity

The boundary conditions in the wet zone are

$$\text{At } x_w = 0 \quad T = T_s$$

$$\text{At } x_w = \delta_w \quad \frac{\partial T}{\partial x} = 0, \text{ or } T = T_\infty$$

As mentioned earlier the coordinate system in the wet zone moves with the recession of the wet/dry interface at velocity $(-V_w)$. Although this region does shrink in size, the part that disappears is at the cold boundary. At this boundary the nodes are allowed to shrink and disappear from the calculation. No special shrinkage terms are included in the calculation because the thermal response of the cold boundary node has negligible impact upon the rest of the problem.

The energy equation is finite differenced semi-implicitly for the end of time step temperature. A semi-implicit formulation is limited in time step size by the Courant condition. However, for most problems this poses no limitation because other factors, such as chemical reaction rate, require a smaller time step.

6.3 The Momentum Equations

The momentum equations in SLAM are in reality very simple; i.e. they have a Darcy's Law form. They relate the motion of a substance, steam, liquid water or air to the pressure gradient and the permeabilities of the porous medium. There are three momentum equations in SLAM, one which governs the flow of gases in the dry zone and two which govern the flow of liquid water and air in the wet zone.

6.3.1 The Dry Zone

The momentum equation in the dry zone can be solved independently of any gas continuity equations because any gas that is formed by evaporation or chemical release will flow to the reaction zone in less time than all other significant changes in the system.

The mass flux of gas at any location is equal to the evaporated flux from the wet/dry interface plus any sources accumulated along the way. Thus

$$\dot{m}(x) = \dot{m}_w + \int_x^{\delta} S \, dx = \frac{-k}{\mu} \frac{P}{RT} \frac{dP}{dx}$$

where

$\dot{m}_w$ = the evaporable water mass flux from the wet/dry interface

k = the permeability (m^2)

μ = viscosity (Kg/m-sec)

P = pressure (pascal)

R = gas constant (m^2/sec^2-K)

T = temperature (K)

S = the source rate of gases (H_2O and CO_2) due to chemically bound release (Kg/m^3)

Rearranging and integrating yields the pressure at the wet/dry interface

$$P_s = \left[P_\infty^2 + 2 \dot{m}_w \int_0^\delta \frac{\mu RT}{k} dx + 2 \int_0^\delta \frac{\mu RT}{k} \int_x^\delta S dx' \, dx \right]^{1/2}$$

The integrals above are carried out numerically. The pressure at any location within the dry zone can be evaluated from the same equation simply by changing the limit of the outer integrals from δ to the desired location.

6.3.2 The Wet Zone

The wet zone momentum equations must be solved simultaneously with the continuity equations for water and air. At any location within the wet zone the pressure is determined by the amount of air present within the voids. The volume of the voids is determined by the total porosity less the volume occupied by the water. If the temperature is high the pressure is the sum of the air pressure plus the steam pressure. If the available void volume shrinks to zero then the pressure distribution is assumed to be determined entirely by Darcy's Law applied to incompressible liquid water. In this case the pressure distribution is simply a linear interpolation between the locations where the pressure is defined by air and steam pressures. The liquid water velocity is uniform for the case where the voids are completely filled with water. In contrast if voids are present the material velocity is determined by the local pressure gradient.

Thus at any location in the wet zone the material velocity V_m is determined by

$$V_m = \frac{-k}{\mu} \frac{dP}{dx}$$

where k is the permeability and μ is the material viscosity.

The pressure at any location is determined by the air density and steam pressure in the available void volume

$$P = \frac{\rho_A RT}{(\varepsilon - \alpha_1)} + P_s$$

where

α_l = liquid water volume fraction = ρ_{H_2O}/D_{H_2O}

P_s = water saturation pressure at temperature T

ε = porosity

ρ_A = the macroscopic air density

T = the temperature from the energy eqn (sec6.2.3) solution

The solution procedure is carried out in four steps, three of which are iterative. Step 1 is to solve the energy equation for the temperature distribution. Step 2 a pressure distribution is evaluated based upon temperature and the air-water-void distribution. Step 3 the velocities of air and water are calculated from Darcy's law. Step 4 the continuity equations for air and water are updated with the velocities from step 3. An error check is made and steps 2,3,4 are repeated until a solution of adequate convergence is obtained.

7. Constitutive Relationships and Miscellaneous

The three sections above describe the system of conservation equations in SLAM. The equations described above cannot be solved without a set of relationships that couple the equations together. In this section the required relationships will be discussed.

7.1 Chemical Kinetics and Heat Generation

The sources/sinks due to chemical reaction are calculated from a general chemical reaction equation of the form

$$aA + bB \longrightarrow cC + dD + \ldots$$

The assumed chemical kinetics equation is

$$\frac{dX}{dt} = A_k e^{-E_k/RT} (X - \rho_A/aW_A) (X - \rho_B/bW_B)$$

Where X is the amount of A or B that has been consumed in reduced molar units, and ρ_A/aW_A is the driving force of material A,

$A_k e^{-E_k/RT}$ is a kinetics rate coefficient of reaction k. In finite difference form the equation becomes

$$\frac{X^{n+1}-X^n}{\Delta t} = A_k e^{-E_k/RT} \left(X^{n+1}-\rho_A/aW_A\right) \left(X^{n+1}-\rho_B/bW_B\right)$$

the value of X at the end of the time step is found from the quadratic formula

$$X^{n+1} = \frac{-B' \pm (B'^2 - 4A'C')^{1/2}}{2A'}$$

where $B' = -(\rho_A/aW_A + \rho_B/bW_B + 1/(A_k e^{-Ek/RT} \Delta t))$
$A' = 1.$
$C' = (\rho_A/aW_A)\ (\rho_B/bW_B)$

When the end of time step value of X^{n+1} is known then the final density of the reactants and products can be calculated from the formulas;

$$\rho_A^{n+1} = - a W_A X^{n+1} + \rho_A^n$$

$$\rho_B^{n+1} = - b W_B X^{n+1} + \rho_B^n$$

$$\rho_C^{n+1} = c W_C X^{n+1} + \rho_C^n$$

$$\rho_D^{n+1} = d W_D X^{n+1} + \rho_D^n$$

Where X^n has been set to zero because only the change in X is of concern.

The heat release (or absorbtion) due to the chemical reaction can be calculated from the first law of thermodynamics for a chemically reacting system.

$$Q_v = \left[\sum n_p \, (H_{fp} + h_p) - \sum n_R \, (H_{fR} + h_R)\right] \frac{X^{n+1}}{\Delta t}$$

where n_R is the reactant coefficient

n_p is the product coefficient

H_f is the heat of formation of the material at the standard state

h is the actual enthalpy of the material at the reaction temperature relative to the standard state

Q_v is the volumetric heat source ($J/m^3 sec$)

7.2 The Chemical Reactions

Concrete consists of a mixture of sand, aggregate, cement, water plus a few other materials that aid in curing. Each of these materials, in turn, consists of a mixture of several different chemicals (except of course water). For example, limestone concrete contains mixtures of dolomite, calcite, orthosilicates, aluminates, clays and a variety of other complex minerals. Sodium can react with possibly all of the different chemicals to some extent, leading to a system of chemical reactions that is extremely complicated. However as far as the model is concerned, only those reactions that have a major impact upon the heat balance, ablation rate, and reactant diffusion need be of concern. Therefore the chemical reactions for limestone concrete have been simplified to the following set:

1) $H_2O + Na \longrightarrow NaOH + 1/2\ H_2$

2) $CO_2 + 2\ Na \longrightarrow 4Na_2O + C$

3) $3CaCO_3 + 4\ Na \longrightarrow 2Na_2CO_3 + 3CaO + C$

4) $3MgCO_3 + 4\ Na \longrightarrow 2Na_2CO_3 + 3MgO + C$

5) $2NaOH + CaCO_3 \longrightarrow CaO + H_2O + Na_2CO_3$

6) $2NaOH + SiO_2 \longrightarrow Na_2SiO_3 + H_2O$

Other possible reactions, such as those which form Na_4SiO_4, have been ignored because silicates are not present in large enough quantities in limestone concrete to provide a significant heat source in comparison to the carbonates.

7.3 The Mass Exchange Coefficients

The mass exchange coefficients are utilized in the continuity equations to model the diffusion of a material due to turbulent mixing. The mixing occurs primarily due to agitation of the pool by the escaping H_2 and Na gases. The gases are expected to cause large scale convection in the pool which will result in fairly good mixing. The convection diminishes near a solid boundary such as the concrete interface. It does not disappear completely at a solid boundary because gases emerge from the concrete and they will stir the materials locally due to entrapment in the wake of the rising bubbles. Therefore it is expected that the mass exchange coefficient that governs these phenomena should have a significant position dependence. Unfortunately an effective mass exchange coefficient that governs phenomena like those described above has not been measured, therefore one is left with selecting a number and its position dependence that best simulates the behavior that is observed experimentally.

Since the SLAM formulation is one-dimensional, it is possible to derive a crude dependence of the mass exchange coefficient upon the gas velocity. The mixing of materials results from motion upward at one location and an equivalent volumetric flow downward at another in order to conserve total volume at any horizontal location. If U is the average upward and downward velocity of material then a finite-difference formulation of the advective continuity equation

$$\frac{\partial \rho}{\partial t} + U\frac{\partial \rho}{\partial x} = 0$$

can be simulated by an equivalent diffusion equation

$$\frac{\partial \rho}{\partial t} = \frac{\partial}{\partial x}\gamma\frac{\partial \rho}{\partial x}$$

if the mass exchange coefficient has the value

$$\gamma = \frac{U\Delta x}{2}$$

where Δx is the finite-difference node size.

For material that is dragged along in the wake of rising bubbles the average upward velocity (U) is proportional to the superficial gas velocity V_g times the bubble velocity V_b [11].

The bubble velocity V_b is assumed to be governed by Stokes law.

$$V_b = \frac{2\, r^2\, \rho\, g}{9\, \mu}$$

where r is the bubble radius

g is gravitational acceleration

ρ is the mixture density

μ is the volume weighted mixture viscosity

In addition to wake transport of material, large convective cells will be set up that have an average velocity (U) that is proportional to the superficial gas velocity. Since the effect of large circulation cells drops to zero at any solid boundary, an exponential dependence was arbitrarily chosen to simulate this dependence.

Thus by substituting and summing the effects mentioned above the final form for the mass exchange coefficient is

$$\gamma(x) = \gamma_\infty \Delta x + \gamma_o V_g V_b \Delta x \,(1 + \gamma_1\,(1-e^{-\gamma_2 x}))$$

where γ_∞, γ_o, γ_1, γ_2 are user input constants, and x is the distance from the concrete interface.

γ_∞ allows the user to input a constant mass exchange coefficient that is independent of position and gas fluxes. γ_o allows the user to adjust the strength of the bubble wake drag. γ_1 and γ_2 allow the user to vary the strength of mixing due to convection within the pool.

The penetration rate is determined by both the magnitude of the mass exchange coefficient and the thickness of the boundary layer. The thickness of the boundary layer is chosen by the user as some fraction of the dry zone. In turn, the dry zone thickness varys with the penetration rate in a reciprocally related fashion. Although this development seems to be getting somewhat complex , it turns out that the competing effects cancel out because of the Δx multiplier in the mass exchange coefficient formula. Although the continuity equation solution does depend upon the choice for the boundary layer thickness fraction, the dependence turns out to be weak because of the effect of the γ_1 and γ_2 coefficients. These coefficients cause the materials to be well mixed away from the interface, and therefore the concentration distribution is independent of the boundary layer thickness (which is user selected). It should be noted that the boundary layer thickness must be chosen to be thick enough so that the solution becomes independent of the fraction chosen. A number of SLAM calculations indicate that boundary layer fractions on the order of 1/3 to 1/2 of the dry region are thick enough for good solutions. In the calculations that appear in this report a boundary layer fraction of 0.42 was used.

The mass exchange coefficients are chosen in an iterative fashion by the user where many calculations are compared with a number of experiments. Further model development in this area is needed such that the mass exchange coefficients would only be a function of the physical properties of the system.

7.4 Variable Thermal Conductivity

Variations in thermal conductivity in sodium-concrete ablation problems are very large. The variations will go from the high conductivity of liquid sodium ~50 w/m·k to the low conductivity of hot dehydrated concrete ~0.1 w/m·k or even lower if vapor phase activity is occurring. Including the variable conductivity is essential if the proper thermal and chemical response of the system is to be calculated.

In the reaction zone the rate of chemical reaction, and its consequent heat production, is a function of the reactant concentration and the temperature. If the thermal conductivity is high, such as when a significant amount of liquid sodium is present, then any heat that is generated will be conducted away rather than causing a temperature rise. In contrast, if the thermal conductivity is low, high temperature and reaction rates will result and this could lead to reactant depletion which terminates the interaction. Thus the behavior of the sodium concrete interaction is very sensitive to the thermal conductivity of the reaction zone.

The thermal conductivity of the reaction zone (boundary layer) is a function of the materials that are present. In turn, the materials that are present depend upon other phenomena such as chemical reaction, turbulent diffusion, and the ablation rate. Thus changing a single parameter, such as the mass exchange coefficient, can lead to a calculated behavior that is significantly different than what may be expected.

A number of SLAM calculations have indicated that the response of the sodium concrete interaction is very sensitive to the mixture rule that is used in calculating the thermal conductivity. Several mixture rules were tried, but most of them resulted in temperatures that were too low when compared to experiment.

In the current version of SLAM a simple volume fraction weighting method of calculating the thermal conductivity has been found to give the best agreement with experimental data.

$$K_{mix} = \alpha_l \sum (\alpha_i \ (K_i + \gamma \rho_i C_i)$$

where α_i is the volume fraction of material i

α_l is the liquid volume fraction

K_i is the thermal conductivity of material i

ρ_i is the macroscopic density of material i

C_i is the specific heat of material i.

γ is the local mass exchange coefficient

The term $\gamma \rho_i C_i$ accounts for the turbulent mixing of the materials. This term assumes that the turbulent Schmidt number is equal to 1.

7.5 Source Term for CO_2 and H_2O Gas Release

The heat that is generated in the reaction zone is partially conducted into the concrete. When the concrete temperature reaches a few hundred degrees Celcius, chemically bound H_2O is released from the cement paste. As temperatures are raised higher, CO_2 gas is released from the complex calcium and magnesium carbonates that are present. The gas release mechanism is actually an imbalance between the rates of absorption and release. The rates are a function of temperature and pressure. If only the release rate is used and the pressure effect ignored, a simple formula will result. The formulas for water release and $CaCO_3$ decomposition are the same as those in the USINT code[13].

The formula for $MgCO_3$ decomposition is estimated from the $CaCO_3$ formula with the understanding that it decomposes at a significantly lower temperature[4].

$$S_{CO_2} = \rho_{CaCO_3}\ 3.3 \times 10^5\ e^{-19362/T} \qquad (CaCO_3)$$

$$S_{CO_2} = \rho_{MgCO_3}\ 4.2 \times 10^8\ e^{-19362/T} \qquad (MgCO_3)$$

$$S_{H_2O} = \rho_{H_2O}\ 3.3 \times 10^{10}\ e^{-20560/T} \qquad (\text{Bound water})$$

where

S is the release rate in Kg/m^3 sec

ρ is the macroscopic density of the bound gas, or binding material.

T is the temperature in degrees Kelvin.

All of the above formulas cause the concrete to degas at any temperature. However, the rate of decomposition is much too slow to be detected at low temperatures. For sodium concrete calculations, the formulas are quite adequate because of the high temperatures and short time scales of the calculations. Finally, it is possible to put in the reverse adsorbtion reactions if problems are encountered where the forward reactions lead to unphysical results.

7.6 The Ablation Rate

The assumed ablation mechanisms in SLAM are dissolution or chemical reaction. The user can choose which mechanism is operative.

7.6.1 Ablation by Dissolution

Dissolution occurs whenever a soluble material is placed in a solvent. At the interface, the material dissolves to it's saturation point and is then transported away by diffusion. In SLAM it is assumed that free NaOH is the solvent and solid $CaCO_3$ is the solute. Thus the formula for the ablation rate is

$$V = \frac{1}{\rho_c} \gamma \frac{\partial \rho}{\partial x}$$

where V is the ablation rate

ρ_c is the macroscopic density of $CaCO_3$ in the concrete at the interface

γ is the mass exchange coefficient at the interface

$\frac{\partial \rho}{\partial x}$ is the concentration gradient of $CaCO_3$ at the interface.

In finite-difference form the equation becomes

$$V = \frac{2}{\rho_c} \frac{\gamma}{\Delta x} (\rho_{Sat} - \rho_i)$$

where Δx is the node width

ρ_i is the macroscopic density of $CaCO_3$ in the node adjacent to the interface

ρ_{Sat} is the macroscopic density of $CaCO_3$ dissolved to its saturation point in the free NaOH.

γ is the diffusivity at the interface

The free sodium hydroxide is that which remains undissolved in the liquid sodium. The macroscopic density of sodium hydroxide is calculated by its continuity equation. Some fraction of the calculated NaOH is dissolved in the liquid sodium. For simplicity it is assumed that the fraction is a constant, generally 5 to 20%, and is user input. Therefore the concentration of free sodium hydroxide is

$$\rho_{l,NaOH} = \rho_{NaOH} - f \rho_{l,Na}$$

where

$\rho_{l,NaOH}$ is the concentration of free NaOH

ρ_{NaOH} is the local concentration of NaOH

f is a user input constant

$\rho_{l,Na}$ is the local concentration of liquid sodium.

The saturation concentration of $CaCO_3$ dissolved in the free NaOH depends upon the $Na^+, Ca^{++}, OH^-, CO_3^{--}$ phase diagram. A small portion of the phase diagram has been measured[15]. A linear fit

to the experimental data for the solubility of $CaCO_3$ in NaOH to 20 mole % yields

$$\rho_{Sat} = \frac{\rho_{l,NaOH} \, W_{CaCO_3} \, F}{W_{NaOH} \, (1-F)}$$

$$F = 3.8 \times 10^{-4} \, T - 0.23294 \text{ if } T < 823 \text{ K.}$$

For solubilities greater than 20 mole % the phase diagram must be assumed. For flexibility and simplicity the following formulation is chosen.

$$F = (1 - e^{-r/(T-823)}) \, 0.9202 + 0.0798 \quad \text{if} \quad T > 823 \text{ K}$$

By varying the input constant r the user can vary the phase diagram in an exponential manner. The numerical constants in the expression above are chosen such that the phase diagram is continuous and covers the full range of miscibility.

In all the simulations that appear in this report the ablation by dissolution option is not used. Calculations indicate that the behavior is quite similar to the ablation by chemical reaction (next section). However, since most of the phase diagram must be assumed, the dissolution option requires unknown parameters to be selected in contrast to the parameter free ablation by chemical reaction option.

7.6.2 Ablation by Chemical Reaction

A second possible mechanism for concrete ablation is chemical reaction. When the concrete at the interface reacts, it is chemically transformed into a liquid slurry and hence penetration is taking place. It is assumed that the rate of chemical reaction is governed by the same chemical kinetics equation that applies in the pool region (sec 7.1) A moving control volume analysis applied to the materials at the interface yields the following formula for the rate of penetration.

$$V = A \, e^{-E/RT} \, \rho_{Na} / W_{Na} a_{Na}$$

where V is the ablation rate

A and E are the kinetic coefficients for calcium carbonate-sodium reactions

W_{Na} is the molecular weight of sodium

a_{Na} is the stoichiometric coefficient for sodium (4)

ρ_{Na} is the macroscopic density of liquid sodium at the interface

For all the simulations in this report the ablation by chemical reaction option is used.

It should be pointed out that the ablation rate (or penetration rate) is not a parameter in the SLAM code, but rather determined entirely by the physics of the ablation rate models described above.

7.7 The Temperature at the Wet/Dry Interface

The interface between the wet zone and the dry zone is the location where the liquid water evaporates. The pressure at this location is governed by the resistance to flow of the evaporated water as it leaves the dry zone. Thus by combining the set of equations that describe the heat fluxes into this interface, the temperature-pressure relationship for saturated water, and the pressure-mass flux relation for flow through the porous dry zone, an interface temperature can be solved for.

The mass flux of evaporated water can be found by an energy balance at the wet/dry interface.

$$\dot{m}_w = \frac{1}{h_{fg}} \left[-K \left[\frac{T_s - T_p}{\delta} + \sum A_m \frac{m\pi}{\delta} \cos(m\pi) \right] + 2\, K_w \frac{T_w(1) - T_s)}{x_w(1)} \right]$$

where subscript w implies wet zone and h_{fg} is the latent heat.

The pressure at the wet/dry interface is the saturation pressure of water at temperature T_s.

$$P_s = P^* \exp(-T^*/T_s)$$

$$P^* = 1.758 \times 10^{10} \text{ pascals}$$

$$T^* = 4500 \text{ K}$$

The T* and P* values were determined by curve fitting the above formula to steam table data.

The pressure at the wet dry interface is also defined by the Darcy equation in Section 6.3.1. Thus a Newton Raphson functional f can be defined which is the difference in the two formulations for pressure, hence the functional

$$f = P_s^2 - P_\infty^2 - 2\dot{m}_w \int_0^\delta \frac{\mu RT}{k}\, dx - 2\int_0^\delta \frac{\mu RT}{k} \int_{x'}^\delta S\, dx'dx$$

is equal to zero at the correct value of T_s.

7.8 The Wet Zone Recession Rate V_w

The maximum pressure in the system is at the wet-dry interface. Thus all flows are away from that location. The wet zone recession rate is equal to the sum of the rate at which the liquid water is moving into the wet zone plus the rate at which the interface recedes due to evaporation. Thus

$$V_w = \frac{\dot{m}_w}{\rho_w(1)} + \frac{k_1 k_{r1}(P_s - P_w(1))}{\mu_1 \quad x_w(1)}$$

$$k_{r1} = \left[1 - \frac{1-\alpha_1}{\varepsilon}\right]^3$$

where

$\dot{m}_w$ is the evaporative water flux

$\rho_w(1)$ is the macroscopic density of water in the first wet zone node

k_1 is the permeability of the concrete

P_s is the pressure at the interface

$P_w(1)$ is the pressure in the first wet zone node

$x_w(1)$ is the width of the first wet zone node

μ_l is the viscosity of water

k_{rl} is a liquid water fraction weighting factor from the USINT code[13]

ε is the porosity

α_l is the volume fraction of liquid water in the first node.

8. SLAM Validations, Simulations and Applications

8.1 Chemical Kinetics Experiment Simulations.

8.1.1 Introduction

A series of laboratory scale chemical experiments have been conducted at Sandia National Laboratories[6]. The experiments were performed in order to develop chemical kinetics correlations that could be used in more comprehensive sodium concrete interaction models.

The experiments were conducted in the following manner. A small crucible, approximately 3 cm in diameter, was filled with 20 g of reactants. The reactants consisted of some combination of limestone concrete and sodium such that the total mass was 20 g. The crucible was then placed in a preheated furnace at 600°C, and the temperature of the reaction mixture was recorded as a function of time. Several tests were run, each time the ratio of sodium to concrete was varied.

In addition, a few calibration tests were executed. The calibration tests consisted of pure sodium, of various masses, heated in the oven in the same manner. Since there were no chemical reactions in the calibration tests, the thermal response was a function only of the thermal mass and heat transfer to the crucible. The calibration tests allow the analyst to adjust the heat transfer parameters in the model thereby isolating the chemical kinetics as the only undetermined parameters.

The SLAM code is set up to model molten sodium overlying concrete. With a few modifications the code is able to model the experiments directly. In doing so only the pool region is retained, and the chemical reaction rate is governed by the reactant concentration only. Although reactant diffusion does occur, as is evidenced by a particle size dependence, it is assumed that this effect can be absorbed into the A_K coefficient described in section 7.1.

The particle size that was used in the experiments was fairly large (~ .5 cm) and was felt to be representative of a sodium-concrete ablation process. Thus it is hoped that the coefficients that were derived from these experiments are accurate in simulating large-scale sodium-concrete interactions.

Among the more important evaluations provided by this series of experiments is the suitability of the chemical kinetics equation (sec. 7.1) in its present form. By varying the ratio of sodium to concrete the full range of driving force is encountered, hence a first order evaluation is possible.

In the simulations the composition of the limestone concrete was assumed to be

H_2O - 5%

$CaCO_3$ - 53.9%

$MgCO_3$ - 23.1%

SiO_2 - 10.5%

inert - 7.5%

8.1.2 Results and Conclusions

A comparison of the calculated and measured temperature-time histories of the simulated experiment appears in figures 3 through 8.

From these experiments, the following constants were derived for the reaction of sodium and limestone concrete.

$CaCO_3 + Na$ $\quad E_k = 60{,}000$ cal/gm-mole

and

$MgCO_3 + Na$ $\quad A_k = 8.85 \times 10^{12}$ if $\alpha_{Na} < 0.6$

$A_k = 8.85 \times 10^{11}$ if $\alpha_{Na} > 0.6$

where α_{Na} = sodium volume fraction

$A_k e^{-E_k/RT} < 0.1$ $\quad (m^3/Kg\text{-mole sec})$

$CaCO_3 + NaOH$ $\quad A_k = 3 \times 10^6$

$E_k = 34{,}000$ cal/gm-mole

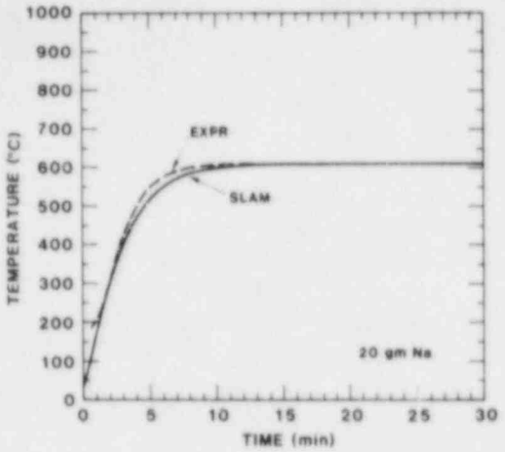

Figure 3. Comparison of SLAM and chemical kinetics calibration test. 20 grams sodium plus 35 gram crucible. There is no chemical reaction in this test.

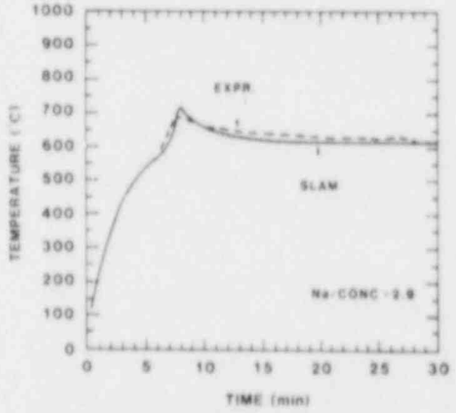

Figure 5. Comparison of SLAM and chemical kinetics test number 2. 5 grams concrete plus 15 grams sodium.

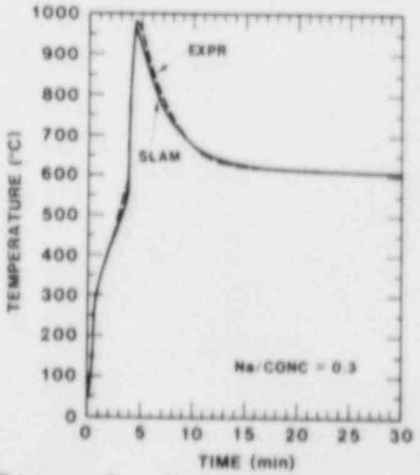

Figure 7. Comparison of SLAM and chemical kinetics test number 4. 15 grams concrete plus 5 grams sodium.

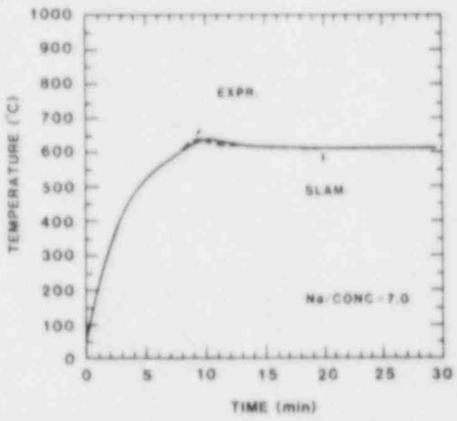

Figure 4. Comparison of SLAM and chemical kinetics test number 1. 2.5 grams concrete plus 17.5 grams sodium.

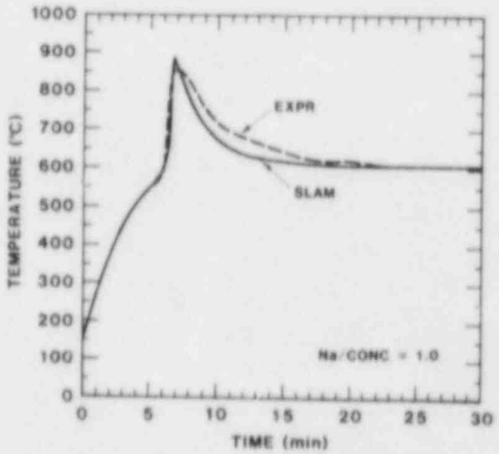

Figure 6. Comparison of SLAM and chemical kinetics test number 3. 10 grams concrete plus 10 grams sodium.

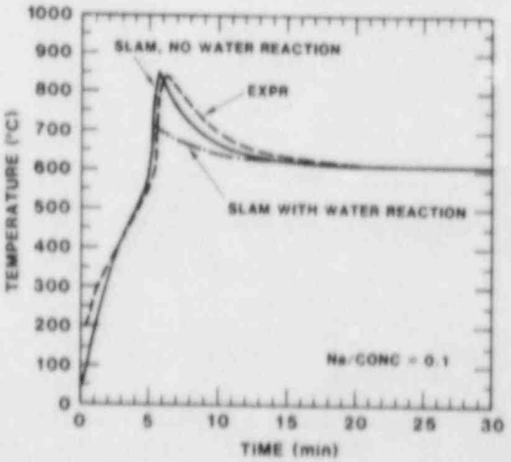

Figure 8. Comparison of of SLAM and chemical kinetics test number 10. 17.5 grams concrete plus 2.5 grams sodium.

The need for using a multi-valued pre-exponential coefficient (A_k) is probably due to a transition from one dominant chemical reaction to another as discussed in reference 6. The transition is not modeled in SLAM because there are only two data points that straddle the transition and more than two unknown parameters would need to be introduced in the correlation.

The accuracy of the sodium hydroxide reaction coefficients is unknown because it was present in such small concentrations that its impact upon the heat balance was overwhelmed by the more dominant sodium-carbonate reactions.

A comparison of the experimental and calculated calibration curves indicates the expected degree of error in the heat transfer simulations. The degree of error in the heat transfer simulations was found to be no larger than the experimental error that results when a calibration test is rerun.

In comparing the experimental vs calculated curves it is found that tests 1, 2, 3, and 4 are in very good agreement when comparing peak size, shape and vertical slope. From these curves it can be concluded that the chemical kinetics model is a suitable one for these types of reactions.

A calculation of test 10 was initially different in peak size. This case was very lean in sodium (2.5 gms) and rich in concrete (17.5 gms). The discrepancy was caused by the sodium reacting with the water that was initially present in the calculation. The water raised the temperature almost instantaneously and consumed a significant fraction of the sodium in doing so. The rapid initial rise in temperature does not occur in the experiments because the water is released at a much higher temperature and over a longer period of time. The second curve was generated by turning off the sodium-water reactions. Without water reactions, excellent agreement is obtained because all of the sodium is available to react with the carbonates when the threshold temperature is reached. The water effects are negligible in the other experiments because significantly less concrete (and its water) was initially present. The water release is correctly accounted for in the whole code because of the existence of the wet and dry zones. (The wet and dry zones were deleted from the code for the chemical kinetics verification simulations).

In conclusion it appears that the simple-model approach is suitable for sodium-concrete kinetics. It is assumed that the kinetics model resulting from these simulations is applicable to large-scale interactions because the experiments were conducted with particle sizes that were felt to be representative of those

that exist in large scale interactions. The driving force of macroscopic molar density divided by the reaction coefficient seems appropriate because it correlates the reaction rate over the full range of sodium density. The resulting coefficients were not single valued but gave the best correlation with experiment if the pre-exponential coefficient A_k was allowed to depend upon the liquid-sodium volume fraction and the total Arrhenius coefficient was not allowed to exceed a value of 0.1 m^3/Kg-mole sec.

8.2 Water Release From Heated Concrete.

Several years ago some water release experiments were conducted at Hanford Engineering Development Laboratories (HEDL)[12]. Among these experiments was WRD-1, in which a right circular cylinder of magnetite concrete was heated at one end for a period of many hours. The rate of water release, and the temperature and pressure at several locations within the concrete block were measured for the duration of the experiment. The results of these experiments are published in reference 12, and they can be compared directly with the SLAM code predictions.

Ideally a comparison of water release from limestone concrete should be compared with SLAM. However data from a similar experiment for limestone concrete does not exist to the author's knowledge. The difference between limestone and magnetite concrete is primarily in the thermophysical properties. The permeability of the two concretes is no doubt different, however, as will be shown, this does not lead to a significant discrepancy in the water release.

Since there are no chemical reactions, and no ablation, only those code modules that calculate water migration and distributions of temperature and pressure can be validated. By setting the A_k's to zero (see 7.1), all chemical reactions will be turned off, and therefore ablation cannot occur. All that remains is to define a pool region of a suitable mass and supply power to it at a rate that matches the boundary condition in the experiment. A calculation of this type has been performed and the results are reported herein.

The thermophysical properties of the concrete are held constant during the calculation in SLAM. In the experiment, the properties are a function of temperature and the degree of dehydration. This difference is expected to cause a deviation in the predicted vs measured response. Thermal conductivity has the greatest variation of all the variables. The variation in thermal conductivity is from 3.75 W/mK at room temperature to 1.25 at the highest temperature (500°C) reached during the course of the calculation (10 hours). In SLAM a constant average

thermal conductivity is used in each region (except in the boundary layer). The conductivity can vary in time, as the average temperature varies, but not space. The same temperature dependence as was chosen for the USINT[13] calculation of the experiment was used in the SLAM calculation.

The thermophysical properties of density (3600 Kg/m^3) and specific heat (800 J/Kg ^oK) are used and held constant throughout the calculation. Although these properties are a function of temperature, their variation is not as great as the thermal conductivity.

The permeability in SLAM does have a temperature dependence. In the dry zone the permeability is assumed to be[12]

$$k = 3.949 \times 10^{-18} \exp(0.0416\ T) \qquad (m^2)$$

and in the wet zone[12]

$$k = 2.94 \times 10^{-28} \exp(0.069\ T) \qquad T < 83\ K$$
$$k = 2.27 \times 10^{-22} \exp(0.0336\ T) \qquad T > 83\ K$$

8.2.2 Results and Conclusions

Thermocouple Traces

Figure 9 displays the measured and SLAM-predicted thermocouple responses at various locations in the concrete. As can be seen from the figures, there is reasonably good agreement. Deviations are seen in the dry zone concrete and this is expected because of the use of constant properties throughout the calculation.

PRESSURE Traces

Figure 10 shows the predicted vs measured pressure response. The predicted pressure has the correct shape but the wrong magnitude at late times. This deviation can be directly traced to an incorrect permeability-temperature relationship in the dry zone. The relationship that is used has too great a permeability at high temperatures. Thus the pressure drop will be too low at late times when the temperature is hotter. The early time pressure response compares very well, most likely because the permeability relationship is reasonable at the lower temperatures.

The deep pressure response shows a considerable discrepancy between the measured and predicted values. This discrepancy is most likely due to experimental difficulties encountered in measuring the pressure as described in ref 12. The SLAM

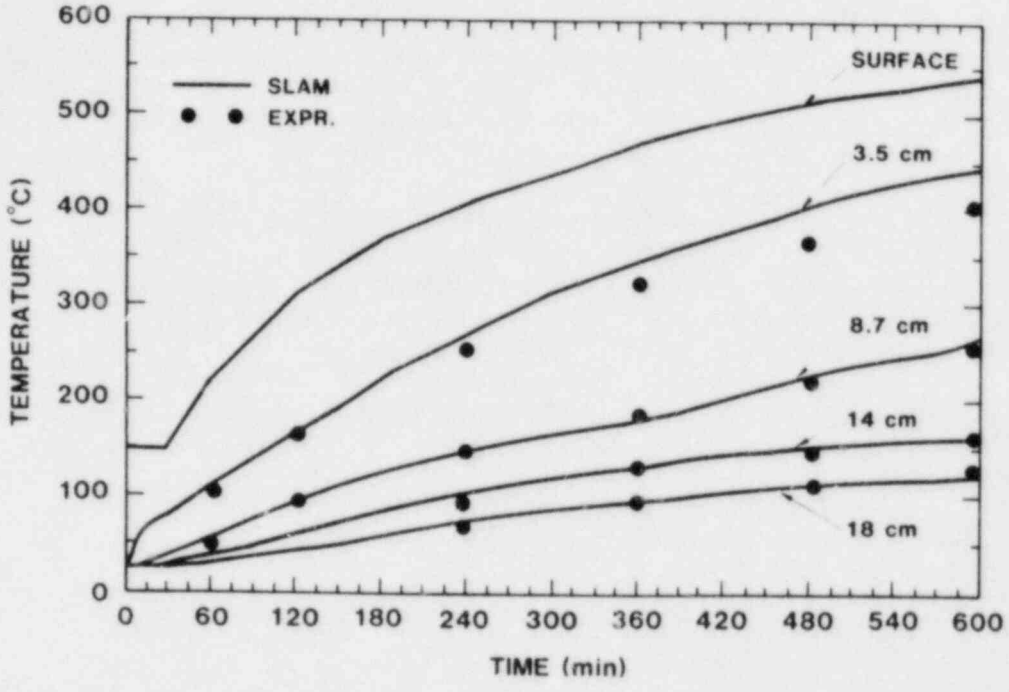

Figure 9. Comparison of SLAM and HEDL WRD-1 test thermocouple data.

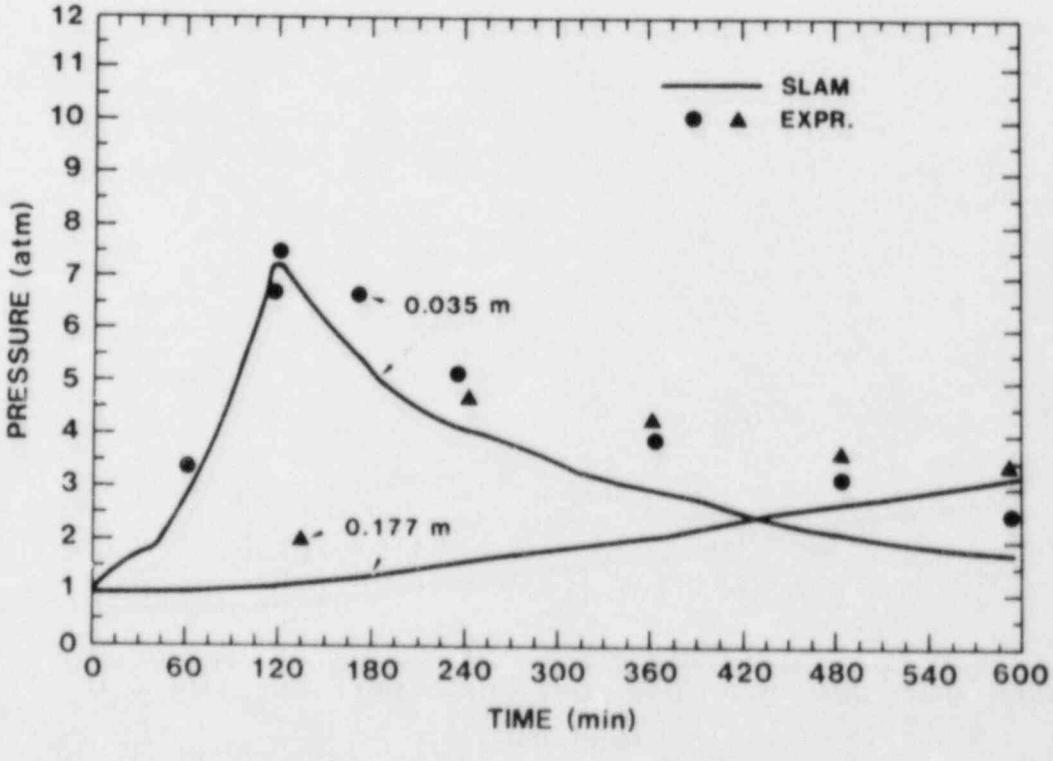

Figure 10. Comparison of SLAM and HEDL WRD-1 test pressure data.

prediction is very similar to the USINT prediction which is expected because the SLAM water migration model is based upon the USINT model, with the major difference being in the numerical methods employed.

Integrated Water Release

The comparison between the measured integrated water release and the predicted water release is shown in Figure 11. Two SLAM predictions are shown. The first uses the water migration as described in Section 6.3.2. As can be seen, excellent agreement is obtained. The second curve corresponds to a fully incompressible assumption for the liquid water within the voids. In using the fully incompressible assumption, the liquid water velocity is simply

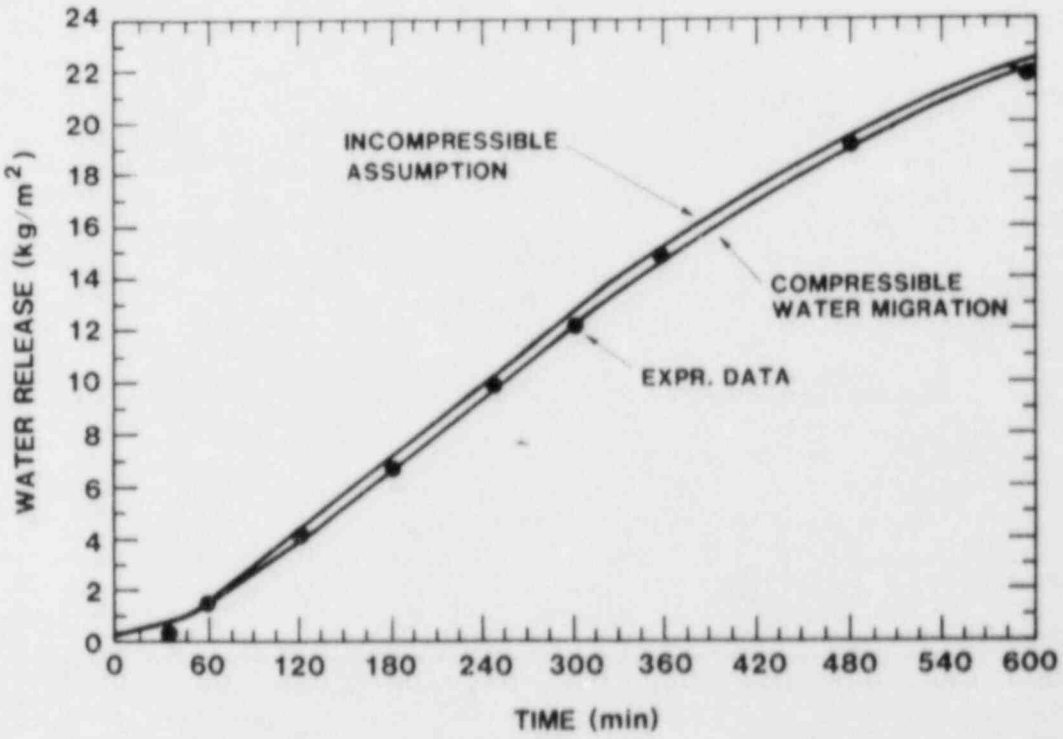

Figure 11. Comparison of SLAM and HEDL WRD-1 test integrated water release. SLAM calculations include the complex (compressible) and simplified (incompressible) water migration solutions.

$$V_w = \frac{\bar{K}(P_s - P_\infty)}{\mu_l \delta_w}$$

where $\bar{K}$ is the average permeability of the wet region
P_s is the pressure at the wet/dry interface
P_∞ is the ambient pressure
μ_l is the liquid water viscosity
δ_w is the thickness of the wet zone.

As can be seen, there is very little difference in the predicted response. This is a very fortunate situation because it implies that the details of the wet zone water migration have very little impact upon the net water release. Thus the simultaneous solution of the continuity and momentum equations in the wet zone (sec 6.3.2) can be deleted altogether, and the equation above used instead. In fact, if the liquid water is assumed completely stationary, the calculated result is not significantly different.

Summary and Conclusions

A calculation was performed of the HEDL WRD-1 experiment to see how well SLAM compares with experimental data. This calculation tests the heat/mass transfer modules for the case of no penetration and no chemical reaction. Results are shown in figures 9-11. Good agreement was found for the temperature response and integrated water release. The pressure response at shallow levels and early times was good but deviated somewhat at late times. The discrepancy is due to an incorrect permeability relationship in the dry zone. The pressure response at deep levels has a large deviation compared to measured values and is due most likely to experimental difficulties, although inadequate modeling of phenomena that occur in the wet zone is also a possibility. The HEDL report stated that there were difficulties in measuring the pressure and that some of the measurements seemed incorrect. In spite of the pressure discrepancies in the wet zone, the amount of water migration is reasonable as evidenced by the good agreement in the integrated water release curve.

As far as sodium-concrete calculations are concerned, the heat/water transfer modules in SLAM are adequate.

Virtually identical results for water release can be obtained by using an incompressible assumption for the liquid water motion. Thus the concrete water migration problems can be modeled with sufficient accuracy if it is reduced to a transient dryout problem and liquid water is treated as incompressible

within the voids. This option has been included in the SLAM code.

8.3 Simulation of Sodium Limestone Experiments

A large number of sodium limestone concrete interaction experiments have been performed to date. Most of these have been at small scale (~1/3 m diameter) and few at large scale (~1 m diameter).

SLAM simulations of these experiments require the use of all parts of the code in a fully integrated fashion. Of the various parts of the code, it is the mass exchange coefficients that lack a comprehensive model. Although there are various functional forms (see Sec. 7.3), there is no direct physical basis for relating the various forms to each other and other properties of the system such as pool depth and aspect ratio. Thus the user is left with selecting numerical values that best simulate the behavior in the experiments.

Of the various functional forms of the mass exchange coefficients (Sec. 7.3), only γ_1 and γ_2 are expected to vary from one experiment to the next. γ_1 and γ_2 represent the mixing due to convective cells that are formed by the viscous drag between the rising H_2 and Na gas bubbles and the liquid slurry. The cell size and velocity depends upon the bubble rise velocity, viscosity, pool depth, shape, and aspect ratio.

8.3.1 Results

Figures 12-14 display the comparisons of the thermocouple traces for Sandia tests SNL-T28 (small-scale)[14], P2-P3 large-scale tests[3] and the AA/AB small-scale test.

In generating these results, the following mass exchange coefficients were utilized

Table 1. The mass exchange coefficients that were used in the SLAM simulations of various sodium limestone-concrete interactions.

All tests	T28	P2	P3	AA/AB
$\gamma_\infty = 10^{-8} m^2/s$	$\gamma_1 = 200$	$\gamma_1 = 200$	$\gamma_1 = 200$	$\gamma_1 = 200$
$\gamma_0 = 0.08$	$\gamma_2 = 0.0$	$\gamma_2 = 2.0$	$\gamma_2 = 2.0$	$\gamma_2 = .04$

As stated earlier, γ_1 and γ_2 vary from one experiment to the next. In the small-scale experiments (T28 and AA/AB), the diameter was 0.3 m and embedded within the pool were heaters and

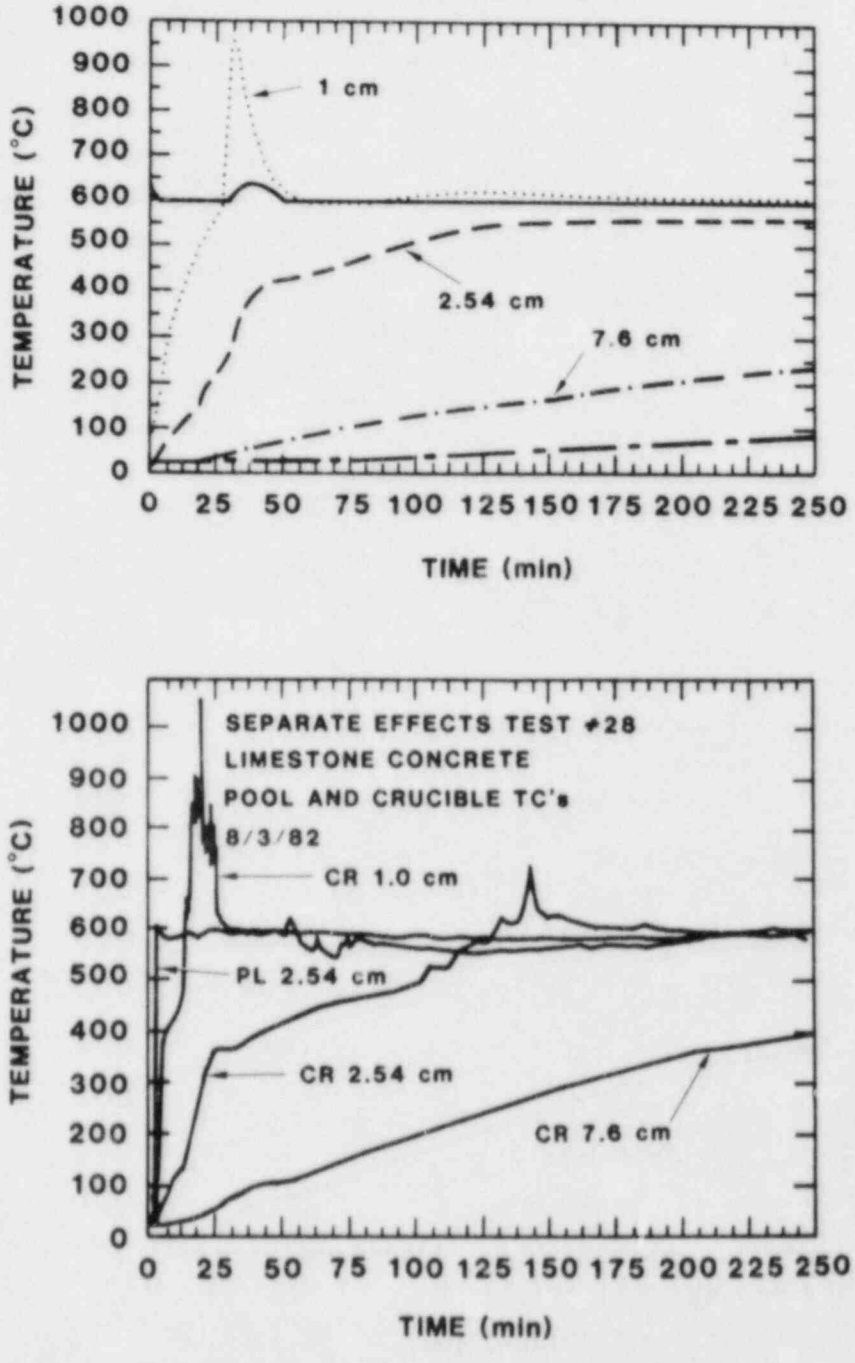

Figure 12. Comparison of thermocouple traces predicted by SLAM and the Sandia small-scale test number 28. The upper figure is the SLAM calculation and the lower figure is the experimental result.

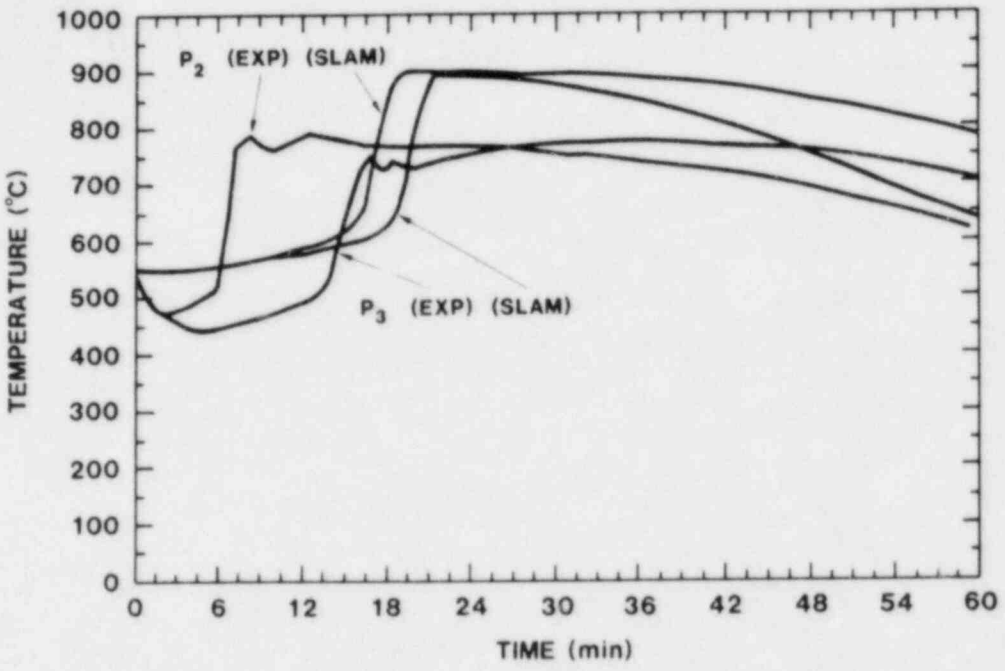

Figure 13. Comparison of the pool thermocouple traces predicted by SLAM and the Sandia large-scale tests P2 and P3.

thermocouple wires. All of these will tend to inhibit convection within the pool, therefore smaller values of γ are used. Tests P2 and P3 were large-scale (approx. 1 m diameter) without pool heaters. The only inhibitory effect upon convection in these tests is the increasing viscosity of the reaction products, an effect that is only crudely modeled in SLAM.

Figures 15-18 display the predicted penetration rates for the same tests. Penetration rates cannot be compared directly, because they cannot be measured in the experiments. The extent of penetration can be compared by post-test examinations, and this comparison is shown in table 2 below:
The AA/AB tests were long-term tests extending in some cases to 20 Hrs. Figures 14 and 18 shows the predicted thermocouple traces and penetration rate as a function of time.

8.3.2 Discussion and Conclusions

Tests T28, P2 and P3 show reasonably good agreement with experiment. This is attributed to SLAM modeling the Phase II part of the interaction. The AA/AB tests have a very different

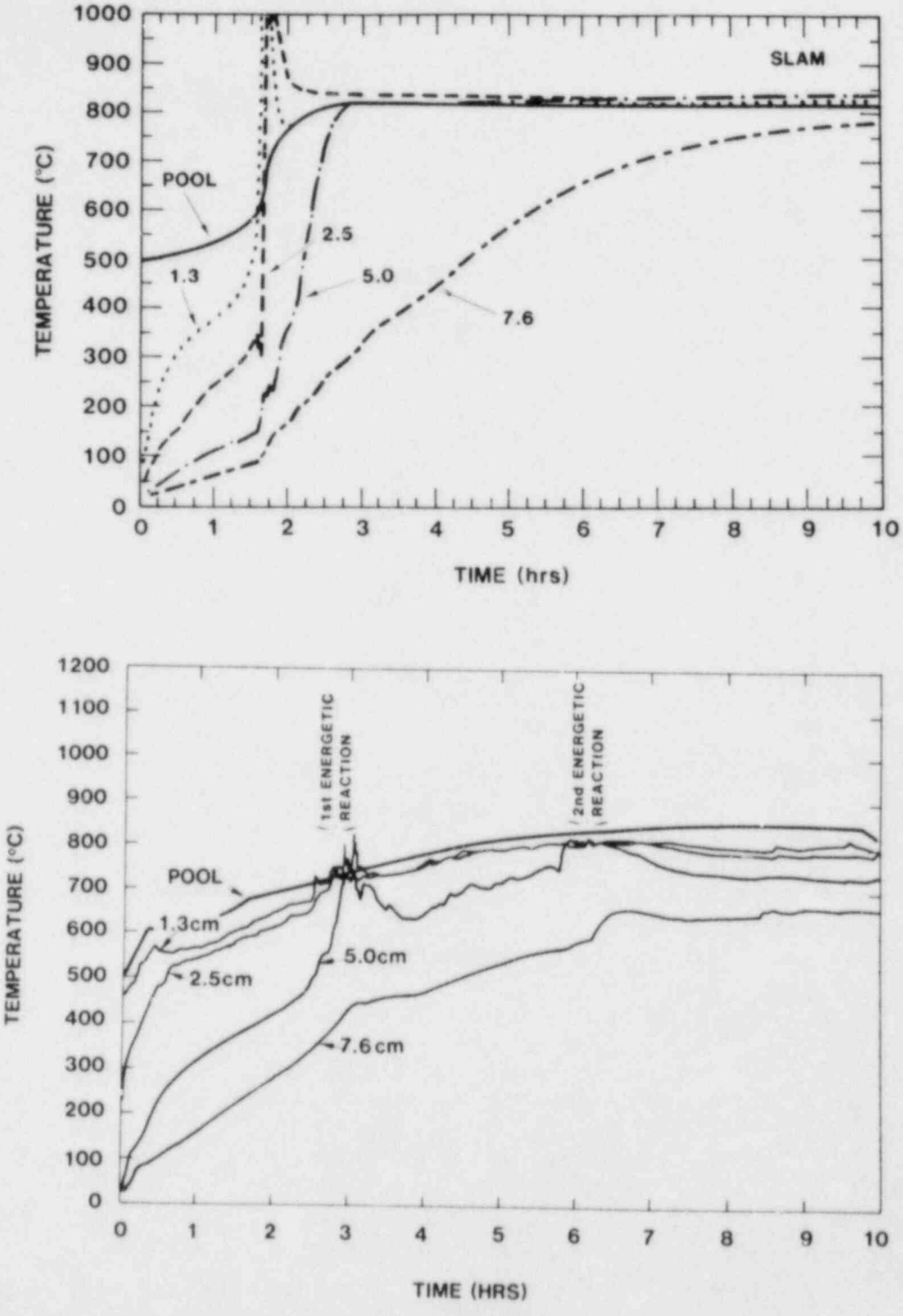

Figure 14. Comparison of the thermocouple traces predicted by SLAM and the Sandia AA/AB calcite test. The upper figure is the SLAM calculation and the lower figure is the experimental result.

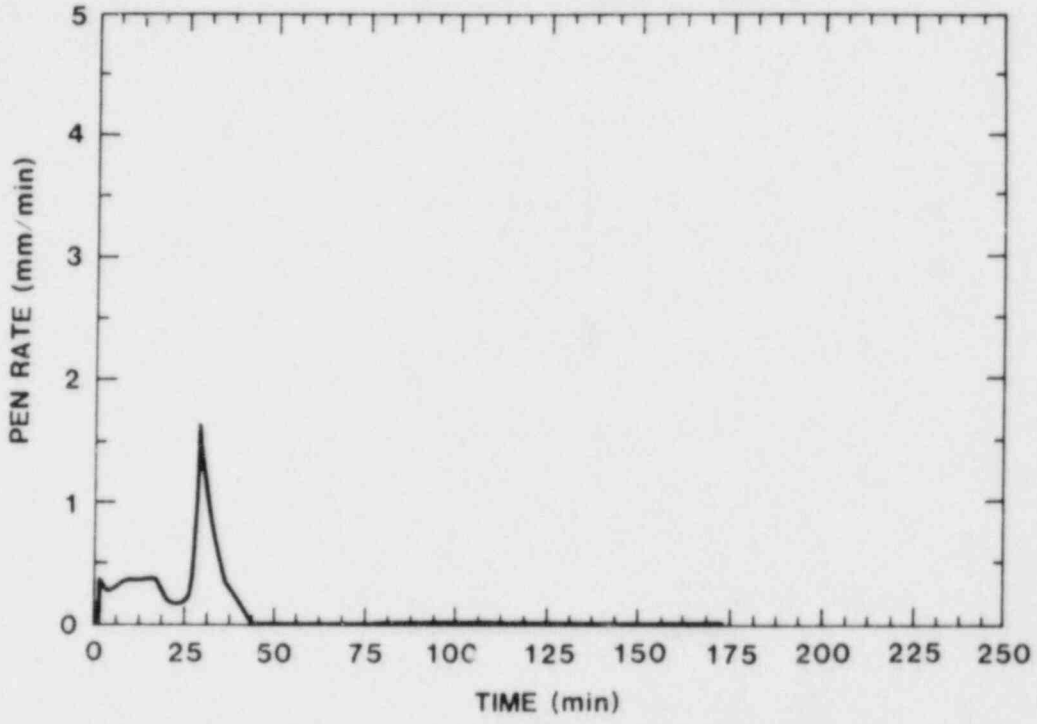

Figure 15. The predicted penetration rate for the Sandia small scale test number 28.

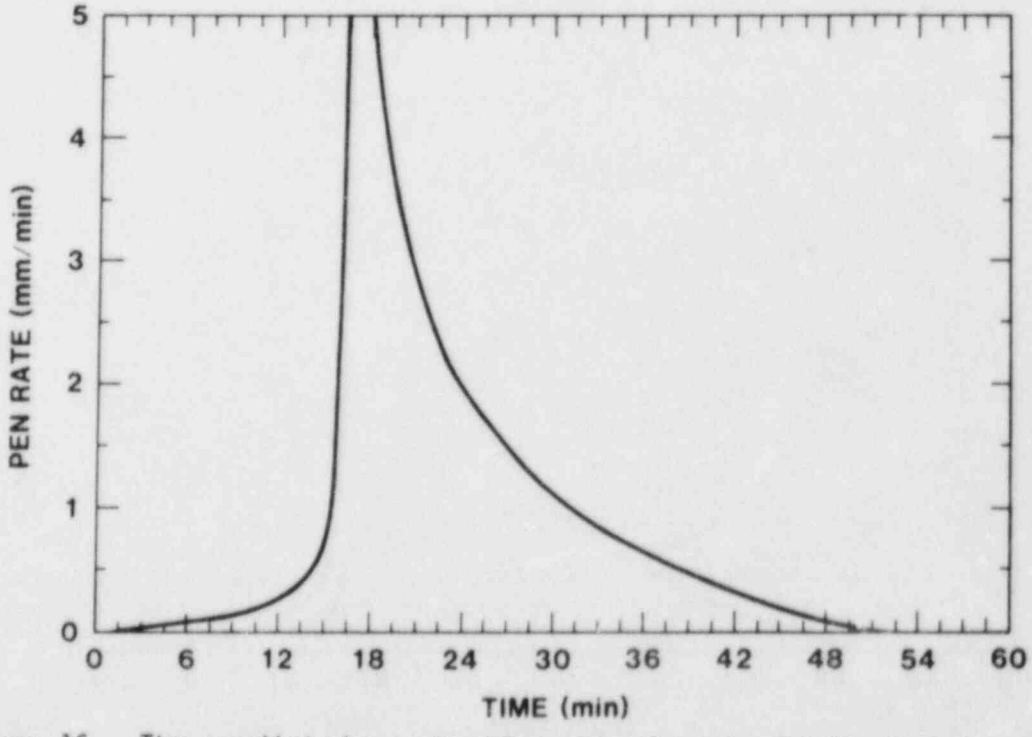

Figure 16. The predicted penetration rate for the Sandia large scale test P2.

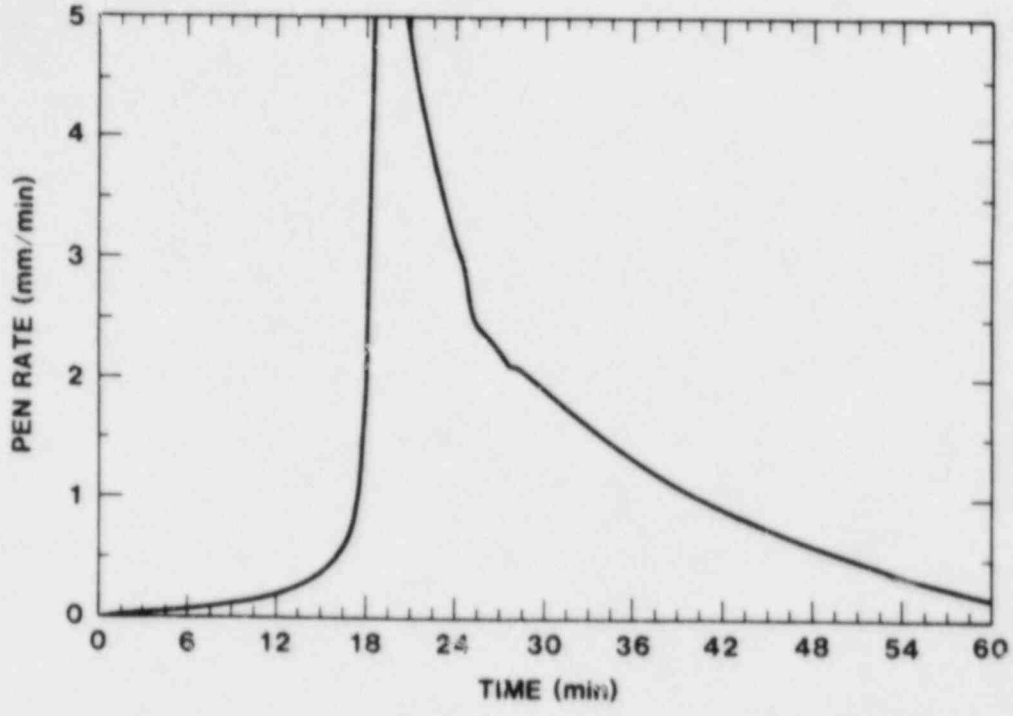

Figure 17. The predicted penetration rate for the Sandia large scale test P3.

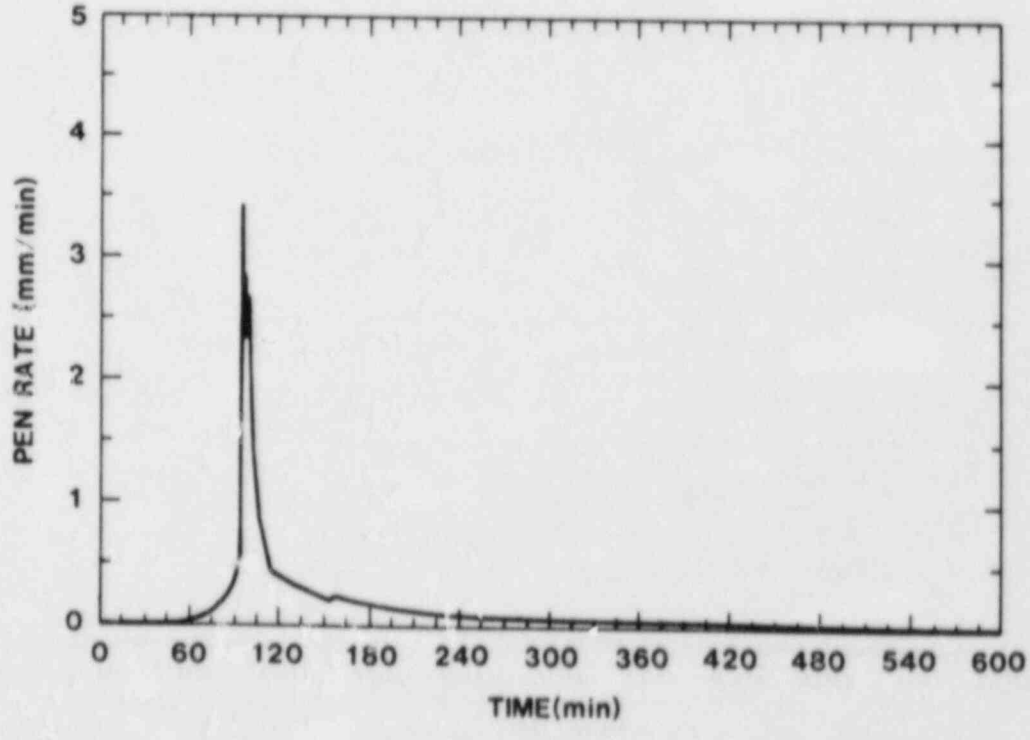

Figure 18. The predicted penetration rate for the Sandia AA/AB calcite test.

Table 2. A Comparison of Measured and Calculated Penetrations in Various Sodium Concrete Interaction Tests.

Test	Total Penetration (m) Measured	SLAM
T28	.042 ± 0.029	.023
P2	.09	.1
P3	.15	.18
AA/AB	.07 ± 0.05	.07

behavior. It seems that the penetration may occur in short cyclic pulses with a period from one to four hours. This behavior is inferred from the irregular thermocouple activity shown in the experimental part of figure 14. All SLAM calculations indicate a direct correspondence between penetration and irregular thermocouple activity. Assuming the same correspondence to occur in the experiment, one is led to the conclusion that the penetration is cyclic, rapid, and of short duration. This behavior is not reproducible with SLAM in its current formulation. It is believed that the cyclic penetration is probably due to a complex interaction of property variations, reaction product settling due to immiscibility and density differences, and sudden fluidization due to the accumulation of gas bubbles within the viscous reaction product layer. Phenomena such as this can be modeled with SLAM if the continuity equation solution technique is modified to account for velocities that are species (and property) dependent.

The extension of SLAM to account for more complex cyclic long-term behavior is not being undertaken at the present time, because it is the vigorous Phase II interaction that seems to pose the greatest safety hazard in LMFBR's insofar as sodium-concrete reactions are concerned.

8.4 Applications

The simulations in the previous sections led to good agreement with experiment. Thus it seems reasonable to apply SLAM to situations that have not been tested yet, at least in a

strictly controlled sense. The effects which can be explored are pool mixing, temperature, and depth. Although many experiments have been performed where these parameters have been varied, it has not been possible to hold the other variables constant and therefore isolate the effect of the phenomenon being investigated.

8.4.1 The Effect of Pool Mixing

The effect of pool mixing in SLAM is simulated by varying the magnitude of the mass exchange coefficient parameters γ_0 through γ_2. Physically, pool mixing is caused by convective cells created by the rising gas bubbles. Therefore for any given experimental conditions a single set of γ's is applicable. By varying the γ's the user can gain an enhanced understanding of how mixing affects sodium concrete interactions.

For the purpose of demonstration, test SNL-T28 will be used as the base case. As mixing is increased, more rapid penetration and heat release is observed. This would normally cause a rapid rise in the pool temperature; however, to isolate the effect of

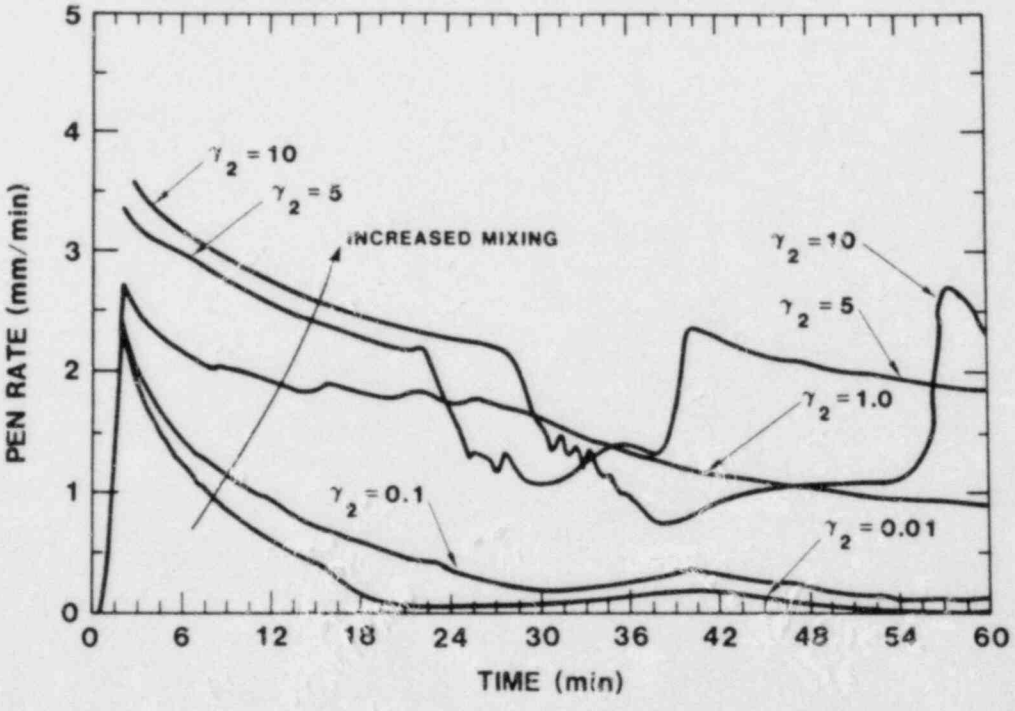

Figure 19. The effect of mixing upon the penetration rate. All other parameters are held constant. γ_2 is defined in the test and has dimensions of m^{-1}.

mixing, the pool temperature was held fixed at the set point of 650°C. Figure 19 shows the effect of mixing upon penetration rate, and Figure 20 shows the effect of the same levels of mixing upon the total extent of penetration. In these simulations only the γ_2 parameter was varied. This parameter simulates the effect of the mixing due to convective cells. Increasing the value of γ_2 simulates a more vigorous cellular flow. From the figures it can be seen that by increasing the level of mixing, a greater penetration rate is observed. This effect is eventually offset by colder interface temperatures due to increased thermal conductivity within the boundary layer. The increased thermal conductivity is caused by a greater concentration of liquid sodium at the interface.

8.4.2 The Effect of Pool Temperature

By holding the initial pool depth and mixing level constant, the effect of pool temperature in isolation can be simulated. Since increased pool temperature leads to enhanced chemical kinetics, a greater rate of penetration is expected. More rapid penetration leads to a greater gas release rate which in turn

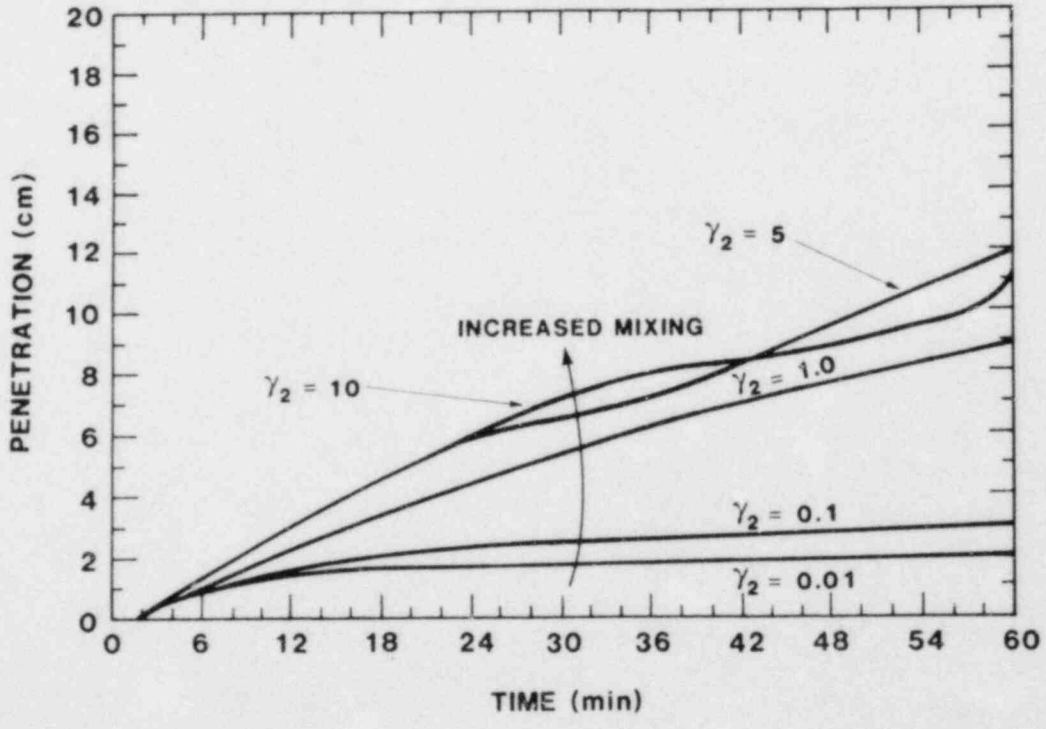

Figure 20. The effect of mixing upon the extent of penetration. All other parameters are held constant.

causes the mass exchange coefficient to vary according to the formula in Sec. 7.3.

In order to prevent superposition of mixing and temperature, $\gamma_{0,1,2}$ were all set to zero and only γ_{∞} was retained. In this simulation the base case does not correspond to any experiment and therefore the variations demonstrate the effect of pool temperature only. Figures 21 and 22 show the effect of pool temperature in isolation. Note that for the 600°C case the penetration rate has a delay time. This is caused by the interface temperature being below the threshold temperature for carbonate chemical reactions. The results for the 700 and 800°C cases are essentially the same. Penetration starts immediately, because the temperature of the interface is above the threshold. This result seems to imply that the phase 1 to 2 transition is related to the concrete-pool interface temperature. The interface temperature is not the same as the pool temperature, because a thermal and composition boundary layer exists between them. Typically the boundary layer is of low thermal conductivity because of the presence of bubbles and other low conductivity materials that displace the high conductivity sodium. Cases with pool temperatures 500°C or below have negligible penetration, because the interface temperature is always below the threshold temperature.

8.4.3 The Effect of Pool Depth. (Sodium Inventory)

Pool depth is a very misleading parameter to vary in isolation because by holding all other parameters constant the only effect will be that of sodium inventory. In reality pool depth affects the mixing level and the pool temperature through its thermal inertia. The effect of all three phenomena simultaneously will be addressed in the next section; therefore, only pool depth as it affects sodium inventory will be addressed in this section. In order to isolate the effect of sodium inventory, a well mixed (fluidized) pool is used. This allows all of the sodium in the pool equal access to the boundary layer. In SLAM this is easily simulated by using a single node, in the pool region. By using a single node the pool region is of uniform composition; hence, termination of the reaction occurs by the combined effects of sodium depletion and dilution of the sodium by the reaction products. Figure 23 and 24 show the effect of pool depth (sodium inventory). As expected the effect is very dramatic for deep pools. Again note that both pool temperature and the mixing level were held constant in this calculation.

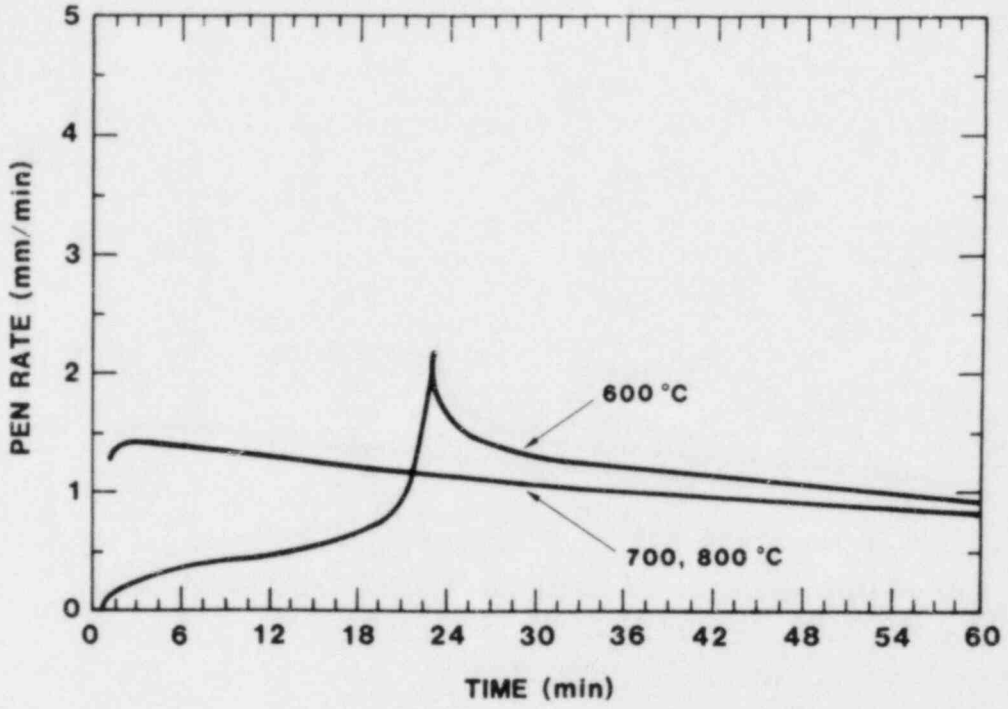

Figure 21. The effect of pool temperature upon the penetration rate. All other parameters are held constant.

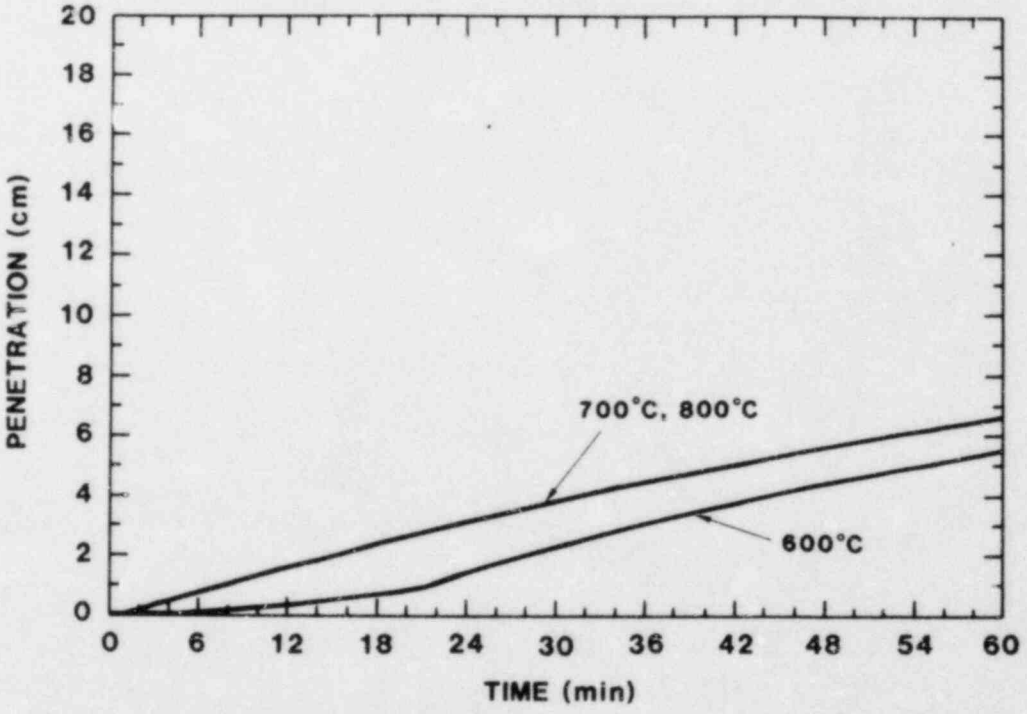

Figure 22. The effect of pool temperature upon the extent of penetration. All other parameters are held constant.

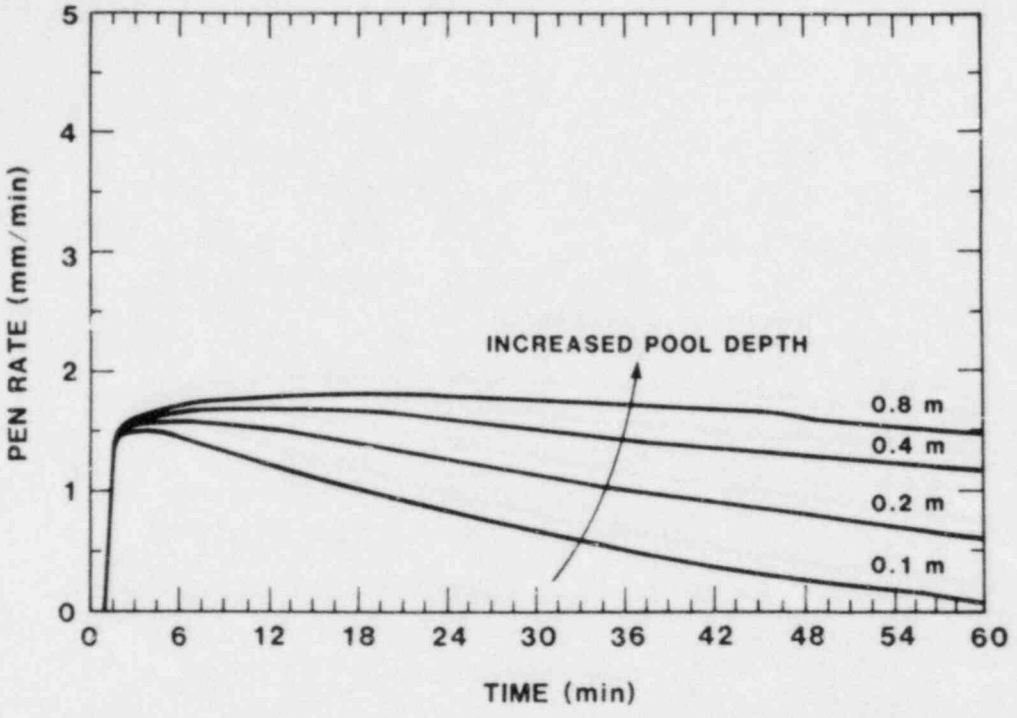

Figure 23. The effect of pool depth (sodium inventory) upon the rate of penetration. All other parameters are held constant.

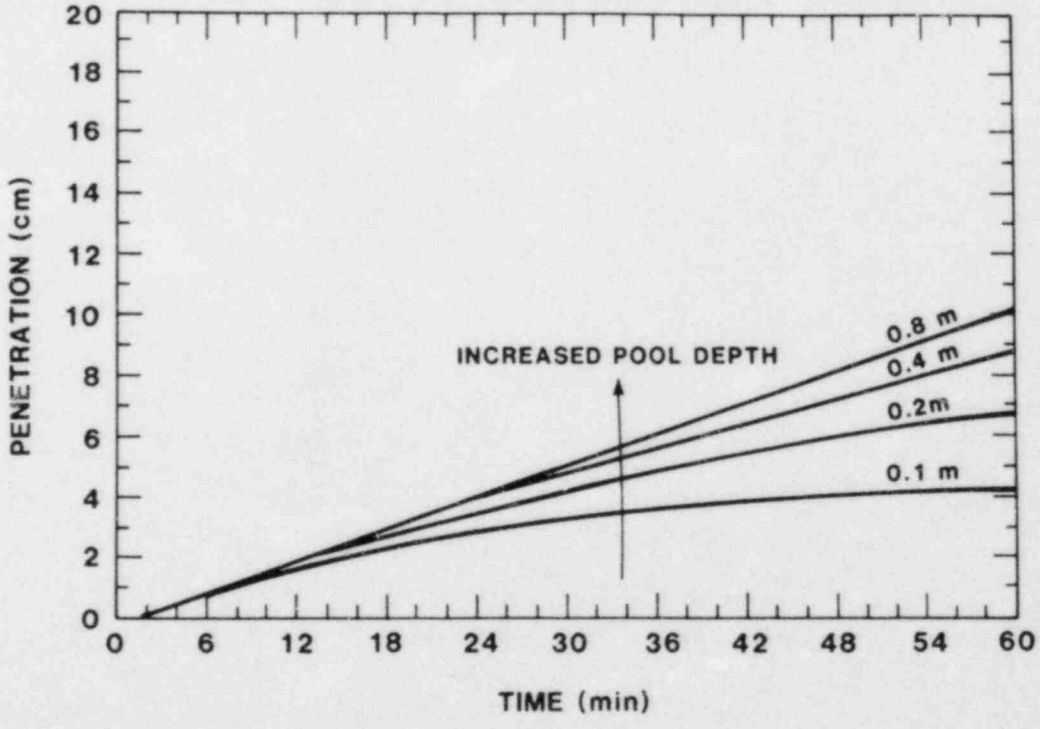

Figure 24. The effect of pool depth (sodium inventory) upon the extent of penetration. All other parameters are held constant.

8.4.4 Very Large Scale Interactions

In this section a preliminary calculation of a very large sodium concrete interaction will be presented. The purpose of the calculation is to give the reader some idea of what the model would predict for a severe accident in an LMFBR. Since the model in its present form is incomplete (that is, it has no comprehensive mass exchange coefficient model), the results should be interpreted as qualitative rather than a quantitative approximation.

There are two main sets of parameters that must be selected for this calculation. The first is the mass exchange coefficient parameters that are appropriate for a very deep pool (5.5 m). The second is the degree of pool fluidization.

The selection of mass exchange coefficient parameters would be automatic if a comprehensive mass exchange coefficient model were incorporated in SLAM. Since such a model isn't available, an arbitrarily chosen mass exchange coefficient based upon table 1 will be utilized. From table 1 the same mass exchange coefficients as were used in the T28 and the AA/AB tests were utilized in the calculations. The P2 and P3 exchange coefficients were not used because the AA/AB coefficients result in a similar though less severe calculation.

Since a fluidization model is also not available in SLAM, it can be simulated by varying the number of nodes in the pool. By using many nodes in the pool the inhibitory effect of a reaction product barrier can be simulated. Conversely by using a single node a completely fluidized pool can be simulated.

Figure 25 shows the predicted penetration rate and extent of penetration for the case with a 5.5m deep pool, 2×10^5 watts/m^2 decay heat, and the mass exchange coefficients mentioned above. As can be seen in figure 25, the maximum rate of penetration is quite large in both cases (T28 and AA/AB). The rate of penetration does decrease to zero after 6 hrs with the T28 coefficients. With the AA/AB coefficients the penetration continues for the entire calculation. The difference in these results indicates how important mixing between nodes in the pool is.

These calculations used 10 composition nodes in the pool region. Physically this corresponds to local fluidization to a .55 m length scale. The penetration rate in these calculations is significantly larger than that which is predicted for the experiments (T28 and AA/AB). The larger penetration rates is caused by having more sodium at the edge of the boundary layer for a greater length of time. The higher sodium concentration is

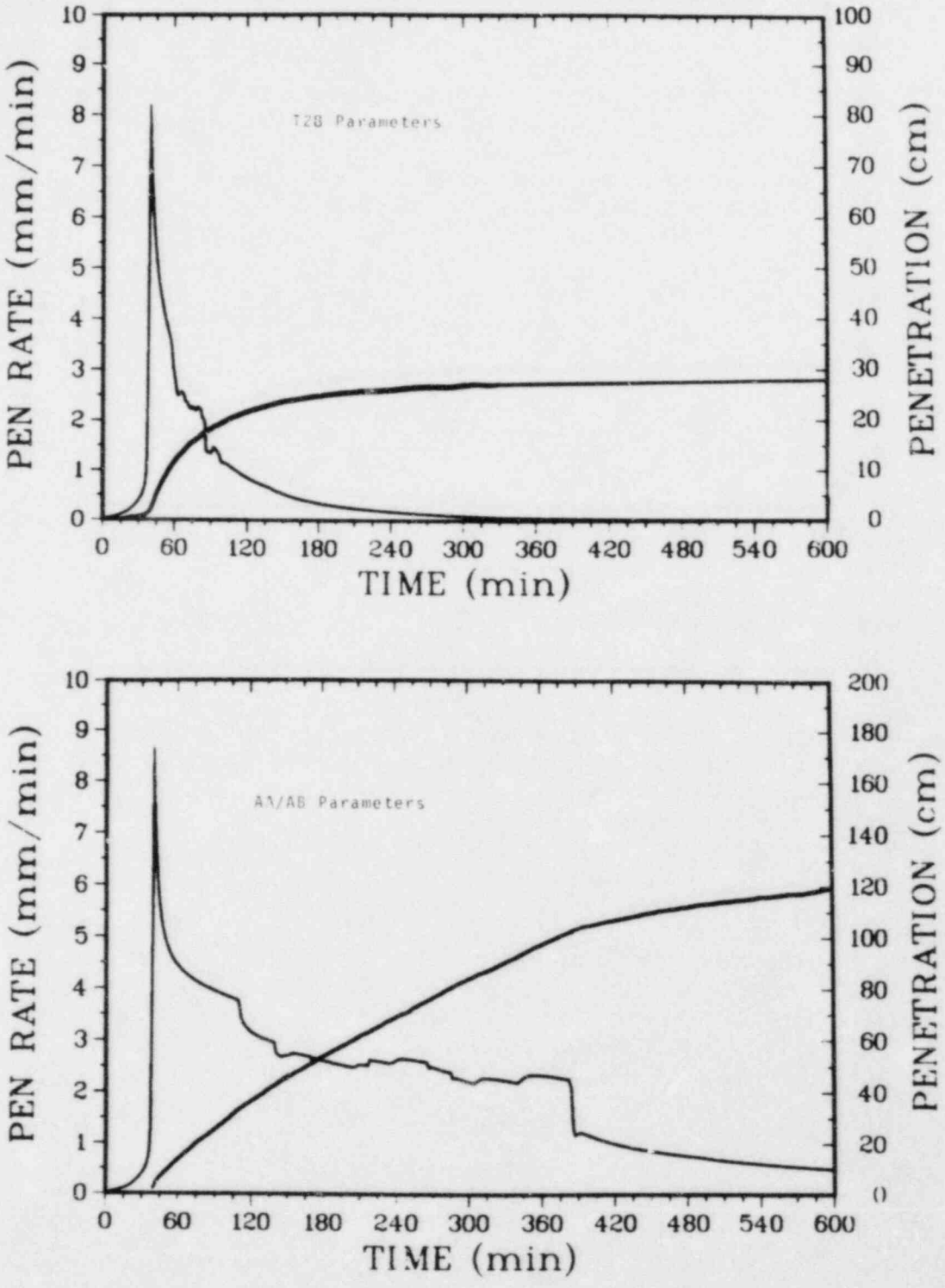

Figure 25. The predicted penetration rate and extent of penetration in a very deep sodium pool with decay heat.

due to the large nodes in the pool (the sodium inventory effect sec 8.4.3). Since these results are significantly different from the experimental results, the model predicts that pool fluidization is the most important parameter in large-scale interactions.

9.0 Summary and Conclusions

The Sodium Limestone Ablation Model (SLAM) is described in detail in this report. SLAM is a three-region model, containing a pool (sodium and reaction debris) region, a dry (boundary layer and dehydrated concrete) region, and a wet (hydrated concrete) region. Each region changes its dimensions and position as time passes. All the important changes are accounted for implicitly in the solution to the system of equations that describe SLAM. Each region consists of a simultaneous solution to the conservation equations of mass, (including chemical species) momentum, and energy. A set of constitutive relationships are included that couple the equations and regions together, so that closed form solutions can be obtained. Of the various constitutive relationships, it is the thermophysical property dependence upon reaction product concentration, penetration rate and other factors that pose the greatest uncertainty upon the results. Of the thermophysical properties, it is the mass exchange coefficients and mixture thermal conductivity that has the greatest impact upon the nature of the solution.

Both isolated as well as integrated "whole code" evaluations have been made with good results. The chemical kinetics and water migration models were evaluated separately, both with good results. Several small and large-scale sodium limestone concrete experiment simulations were made also. The sodium-concrete simulations required user adjusted mass exchange coefficients in order to match the data. This implies the need to develop a mass exchange coefficient model that would predict an appropriate value based upon the pool depth, aspect ratio and extent of reaction.

The SLAM code was applied to investigate the effects of mixing, pool temperature, pool depth and fluidization. All these phenomena were found to be of significance in the predicted response of the interaction.

Appendix A
Thermophysical and Chemical Properties

This appendix includes a list of thermophysical and chemical properties of the materials used in SLAM. Table A1 is a list of the properties for each chemical species that occurs in the pool region and the boundary layer. A set of symbol definitions, a discussion of the properties and a list of sources appears after the table. All material properties are assumed constant except where noted otherwise.

Table A1. Thermophysical and Chemical Properties of the Materials in SLAM

	SiO_2	H_2O	Na	H_2	NaOH	Na_2SiO_3	Na_2CO_3	Na_2O	CaO	$CaCO_3$	CO_2	C	$MgCO_3$	MgO
ρ_i	6.00E+01	1.80E+01	2.30E+01	2.00E+00	4.00E+01	1.22E+02	1.06E+02	6.20E+01	5.60E+01	1.00E+02	4.40E+01	1.20E+01	8.43E+01	4.03E+01
P*	0.00E+00	1.76E+10	3.27E+09	0.00E+00	4.00E+09	0.00E+00	0.00E+00	0.00E+00	0.00E+00	0.00E+00	0.00E+00	0.00E+00	0.00E+00	0.00E+00
T*	0.00E+00	4.50E+03	1.20E+04	0.00E+00	1.75E+04	0.00E+00	0.00E+00	0.00E+00	0.00E+00	0.00E+00	0.00E+00	0.00E+00	0.00E+00	0.00E+00
μ_i	2.00E+00	2.30E-04	1.86E-04	2.00E+00	1.00E-03	2.00E+00	2.00E+00	2.00E+00	2.00E+00	2.00E+00	2.00E+00	2.00E+00	2.00E+00	2.00E+00
D_i	1.20E+03	6.00E+02	8.00E+02	3.00E+03	8.50E+02	1.20E+03	1.20E+03	1.20E+03	1.20E+03	1.20E+03	3.00E+03	1.20E+03	1.40E+03	1.40E+03
T_m	1.74E+03	2.98E+02	3.71E+02	2.98E+02	5.95E+02	1.36E+03	1.12E+03	1.41E+03	2.89E+03	3.00E+03	2.98E+02	2.98E+02	2.98E+02	2.98E+02
T_s	0.00E+00	3.73E+02	1.18E+03	0.00E+00	0.00E+00	0.00E+00	0.00E+00	0.00E+00	0.00E+00	0.00E+00	0.00E+00	0.00E+00	0.00E+00	0.00E+00
H_f	-8.58E+08	-2.86E+08	-2.41E+06	0.00E+00	-4.18E+08	-1.56E+09	-1.13E+09	-4.18E+08	-6.34E+08	-1.21E+09	-3.93E+08	0.00E+00	-1.12E+09	-6.02E+08
h_{fg}	0.00E+00	2.33E+06	3.87E+06	0.00E+00	0.00E+00	0.00E+00	0.00E+00	0.00E+00	0.00E+00	0.00E+00	0.00E+00	0.00E+00	0.00E+00	0.00E+00
h_{sf}	0.00E+00	0.00E+00	1.14E+05	0.00E+00	2.76E+05	3.53E+05	2.79E+05	7.57E+05	0.00E+00	0.00E+00	2.00E+05	0.00E+00	0.00E+00	0.00E+00
K	5.00E-01	1.10E-01	5.00E+01	5.00E-02	5.00E-01	5.00E-01	5.00E-01	5.00E-01	5.00E-01	7.50E-02	5.00E-01	5.00E-01	5.00E-01	5.00E-01
C_s	1.10E+03	0.00E+00	1.30E+03	0.00E+00	3.83E+03	1.49E+03	1.58E+03	1.65E+03	8.77E+02	1.17E+03	0.00E+00	1.24E+03	1.17E+03	8.77E+02
C_l	0.00E+00	4.18E+03	1.30E+03	0.00E+00	3.61E+03	0.00E+00	1.78E+03	1.64E+03	0.00E+00	0.00E+00	0.00E+00	0.00E+00	0.00E+00	0.00E+00
C_g	0.00E+00	1.86E+03	9.04E+02	1.49E+04	0.00E+00	0.00E+00	0.00E+00	0.00E+00	0.00E+00	0.00E+00	1.38E+03	0.00E+00	0.00E+00	0.00E+00

Definitions, Discussions and Sources

W	Molecular weight from a periodic chart of the elements.[16]
P* and T*	Vapor pressure parameters (see Section 7.7.) The numerical values were derived by the author by curve fitting to saturation pressure data.[16]
μ	Viscosity N/m-sec Randich[4] et al. measured the non-Newtonian viscosity of the reaction products resulting from a sodium-limestone concrete interaction as a function of temperature. The measurements did not include the presence of sodium nor did they depend upon the species present. A volume weighted viscosity mixture rule was arbitrarily adopted to account for the presence of sodium and sodium hydroxide.[16] A constant value of viscosity, equal to that measured at high temperatures,[4] is used for all of the remaining chemical species. The volume weighting mixture rule reduces to the measured value when Na and NaOH are not present, and it decreases the viscosity when Na and NaOH are present in significant proportions.
D_i	Slurry microscopic density. In the absence of porosity, D_i would be identical to the published microscopic density for each material. However, measurements of the mass and volume of cold reaction products indicates that porosity is present. Therefore, all materials except sodium have hypothetical microscopic densities that are consistent with measured reaction product volumes and masses. Sodium has its published[16] value of microscopic density.
T_m	The melting temperature[16]
T_S	The 1 atm saturation temperature[16]
H_f	The heat of formation (J/Kg-mole)[16,17,18] at standard conditions. A value of zero in this row indicates the actual value.
h_{fg}	The latent heat of vaporization (J/Kg)[16]
H_{sf}	The latent heat of fusion (J/Kg)[16,17,18]

K — The thermal conductivity. The thermal conductivity of the slurry mixture is unknown. It was assumed to be 0.05 W/mK for all materials except sodium because of similar conductivities for other salts and ceramics. The mixture rule in Section 7.4 accounts for the presence of liquid sodium.

Cs,e,g — The material specific heat for solids (s), liquid (l), and gas (g).[16,17,18] Values of zero indicate that that material does not exist in that phase in the current version of SLAM.

Concrete Properties

Density - 2250 Kg/m^3 [19]

Specific heat - 800 J/Kg-K [19]

Thermal conductivity $K = 1.375 \times 10^{-3}T + 1.6218$ W/m-K

$K \geq 0.1$ W/m-K

Chemical composition - See Section 8.1.1

Permeability - See Section 8.2

Water Content - Free water 110 Kg/m^3

Bound water 72 Kg/m^3

References

1. Postma, A. K., et al., A Review of Sodium Concrete Reactions, HEDL TME 81-7, Dec 1981.

2. Acton, R. U. et al., Molten Sodium Interactions with Basalt Concrete and Siliceous Firebrick, NUREG/CR-0934, SAND79-0938, 1979.

3. Randich, E., et al., Large Scale Exploratory Tests of Sodium/Limestone Concrete Interactions, NUREG/CR-3000, SAND82-2315, 1983.

4. Randich, E., Acton, R., Intermediate-Scale Tests of Sodium Interactions With Calcite and Dolomite Aggregate Concretes, NUREG/CR-3288, SAND83-1064, 1983

5. Barker, M. G., and P. G. Gadd, A Chemical Study of the Sodium Concrete Reaction, Proc. LMFBR Safety Topical Mtg., LYON, France July, 1982. Vol 3, pp 91-107.

6. Westrich, H. R., et al., Laboratory-Scale Sodium-Carbonate Aggregate Concrete Interactions, NUREG/CR-3401, SAND83-1502, 1983

7. Fritzke, H. (GKSS-Geesthacht, West Germany) Personal Communication.

8. Nguyen, D. H., et al., Sodium Concrete Reaction Model Development, Proc. LMFBR Safety Topical Mtg., Lyon France July 1982, vol 3, pp153.

9. Dufresne, J., et al., Sodium Concrete Interaction, Proc LMBFR Safety Topical Mtg., Lyon France, July 1982. Vol 3, pp109.

10. Suo-Anttila, A.., Sodium Concrete Ablation Model, NUREG/CR 2029, SAND81-0415, 1981.

11. Chawla, T. C., and D. R. Pederson, A Review of Modeling Concepts for Sodium Concrete Reactions and a Model for Sodium Transport to the Unreacted Concrete Surface, ANL/RAS 83-8 Apr. 1983

12. McCormack, J. D., et. al., Water Evolution From Heated Concrete, HEDL-TME 78-87. Feb. 1979.

13. Beck, J., and R. Knight, Users Manual For Usint, NUREG/CR-1375, SAND79-1694. May 1980.

14. Advanced Reactor Safety Research Quarterly Report. Oct-Dec 1982,Vol 20.

15. Sallach, R. A., The NaOH-Rich Corner of the (Na^+, Ca^{2+}) (OH^+, CO_3^{2-}) Reciprocal System, NUREG/CR-3269, SAND82-1980

16. Weast, R. C., and M. J. Astle, CRC Handbook of Chemistry and Physics, 62nd edition, 1981-1982.

17. Stull, D. R. , and H. Prophet, Janaf Thermochemical Tables, 2nd edition, June 1971.

18. Bavin, I., and O. Knacke, Thermochemical Properties of Inorganic Substances, Springer-Verley, Berlin, Heidelberg, New York, 1973.

19. Dr. L. Leibowitz. Private communication, October 12, 1979.

DISTRIBUTION:

U. S. NRC Distribution Contractor (CDSI)
7300 Pearl Street
Bethesda, MD 20014
250 copies for R7

U. S. Nuclear Regulatory Commission (13)
Office of Nuclear Regulatory Research
Washington, DC 20555
Attn: O. E. Bassett
B. S. Burson
R. T. Curtis
C. N. Kelber
J. Larkins
M. Silberberg
L. S. Tong
R. W. Wright
T. Walker (5)

U. S. Nuclear Regulatory Commission (6)
Office of Nuclear Reactor Regulation
Washington, DC 20555
Attn: N. Anderson
J. K. Long
J. F. Meyer
A. R. Marchese
T. P. Speis
W. Morris

U. S. Department of Energy (2)
Albuquerque Operations Office
P. O. Box 5400
Albuquerque, NM 87185
Attn: J. R. Roeder, Director
Operational Safety Division
D. K. Nowlin, Director
Special Programs Division
For: C. B. Quinn
D. Plymale

U. S. Department of Energy
Office of Nuclear Safety Coordination
Washington, DC 20545
Attn: R. W. Barber

General Electric Corporation (3)
310 De Guigne Drive
Sunnyvale, CA 94086
Attn: J. W. McDonald, Mgr.
Containment Radiological Evaluation
M. I. Temme, Mgr.,
Safety Criteria Assessments
K. H. Chen, M/C S-54

W. Tarbell
Ktech Corporation
901 Pennsylvania NE
Albuquerque, NM 87110

I. Catton
UCLA
Nuclear Energy Laboratory
405 Hilgard Ave.
Los Angeles, CA 90024

Brookhaven National Laboratories (3)
Upton, NY 11973
Attn: D. Hsieh
T. Pratt

Los Alamos National Laboratory (3)
P. O. Box 1663
Los Alamos, NM 87545
Attn: T. Butler
D. Jensen
A. Neuls

L. Baker, Jr.
ANL
9700 S. Cass Avenue
Argonne, IL 60439

Burns Roe Industrial Services Corp. (2)
650 Winters Ave.
P.O. Box 667
Paramus, NJ 07652
Attn: A. T. Dajani
R. E. Palm

Prof. Charles E. Semler, Director
Refractories Research Center
The Ohio State University
17 Watts Hall
2041 College Road
Columbus, OH 43210

Westinghouse HEDL (3)
P.O. Box 1970
MS W-221T (HE)
Richland, WA 99352
Attn: L. Muhlstein
D. H. Nguyen
J. Carver

Cathy Anderson
Nuclear Safety Oversight Commission
1133 15th Street NW
Room 307
Washington, DC 20005

Battelle Columbus Laboratory
505 King Avenue
Columbus, OH 43201
Attn: J. Gieseke

Wang Lau
TVA
400 Commerce, W9C157-CK
Knoxville, TN 37902

Nuclear Engineering Department (2)
University of Wisconsin
Madison, WI 53706
Attn: M. Corradini
S. Abdul-Kalik

D. Swanson
P. O. Box 214
Hawthorne, CA 90250

M. Fontana
Director, IDCOR Program
Technology for Energy Inc.
P. O. Box 22996
10770 Dutchtown Road
Knoxville, TN 37922

E. Arbtin
EG G, Idaho Inc.
P.O. Box 1625
Idaho Falls, ID 83401

Westinghouse Corp. (2)
Advanced Reactor Division
Box 158
Madison, PA 15663
Attn: L. Strawbridge
T. W. Ball

Westinghouse Corp. (3)
CRBR-P
120 South Jefferson Circle
Oak Ridge, TN 37830
Attn: M. F. McKeown
P. Bradbury
G. Clare

Shu-Chien Yung
HEDL MS W/C - 83
Richland, WA 99352

CRBRP - Project Office (3)
P. O. Box U
Oakridge, TN 37830
Attn: P. J. Gross
C. H. Fox
N. N. Kaushal

Hiroshi Hiroi
PNC/O-arai Engineering Center
4002 Narita, O-arai machi
Higashi-Ibaraki, Ibaraki 311-13
JAPAN

1000 J. K. Galt
1500 W. Herrmann
1540 W. C. Luth
1543 T. M. Gerlach
1543 H. R. Westrich
1543 H. W. Stockman
6313 F. Nimick
6400 A. W. Snyder
6410 J. W. Hickman
6411 A. S. Benjamin
6412 J. W. Hickman, Acting
6413 N. R. Ortiz
6414 G. B. Varnado
6420 J. V. Walker
6421 T. R. Schmidt
6422 D. A. Powers (5)
6422 E. Randich (5)
6423 P. S. Pickard

6425 W. J. Camp
6425 A. Suo-Anttila (5)
6427 M. Berman
6440 D. A. Dahlgren
6442 W. A. Von Riesemann
6443 D. D. Carlson
6444 S. L. Thompson
6448 L. O. Cropp
6449 K. D. Bergeron
6450 J. A. Reuscher
7530 W. E. Caldes
7537 N. R. Keltner
7537 R. U. Acton
8214 M. A. Pound
3141 L. J. Erickson (5)
3151 W. L. Garner

NRC FORM 335 (11-81) U.S. NUCLEAR REGULATORY COMMISSION

BIBLIOGRAPHIC DATA SHEET

1 REPORT NUMBER (Assigned by TIDC and Vol. No. if any)
NUREG/CR-3879
SAND83-7114

2 Leave blank

3 TITLE AND SUBTITLE
SLAM - A SODIUM-LIMESTONE CONCRETE ABLATION MODEL

4 RECIPIENT'S ACCESSION NUMBER

5 DATE REPORT COMPLETED
MONTH December YEAR 1983

6 AUTHOR(S)
Ahti Suo-Anttila

7 DATE REPORT ISSUED
MONTH January YEAR 1984

8 PERFORMING ORGANIZATION NAME AND MAILING ADDRESS (Include Zip Code)
Sandia National Laboratories
Albuquerque, NM 87185

9 PROJECT/TASK/WORK UNIT NUMBER

10 FIN NUMBER
NRC FIN No. A1054

11 SPONSORING ORGANIZATION NAME AND MAILING ADDRESS (Include Zip Code)
Division of Reactor Safety Research
Office of Nuclear Regulatory Research
U.S. Nuclear Regulatory Commission
Washington, DC 20555

12a TYPE OF REPORT
Description of computer model

12b PERIOD COVERED (Inclusive dates)
n/a

13 SUPPLEMENTARY NOTES

14 ABSTRACT (200 words or less)

The Sodium-Limestone Ablation Model (SLAM) is described in detail in this report. SLAM is a three-region model, containing a pool (sodium and reaction debris) region, a dry (boundary layer and dehydrated concrete) region, and a wet (hydrated concrete) region. The model includes a solution to the mass, momentum, and energy equations in each region. A chemical kinetics model is included to provide heat sources due to chemical reactions between the sodium and the concrete.

Both isolated model as well as integrated "whole code" evaluations have been made with good results. The chemical kinetics and water migration models were evaluated separately, with good results. Several small and large-scale sodium limestone concrete experiments were simulated with reasonable agreement between SLAM and the experimental results.

The SLAM code was applied to investigate the effects of mixing, pool temperature, pool depth and fluidization. All these phenomena were found to be of significance in the predicted response of the sodium concrete interaction. Pool fluidization is predicted to be the most important variable in large scale interactions.

15a KEY WORDS AND DOCUMENT ANALYSIS

15b DESCRIPTORS

Sodium-concrete interactions, sodium-interactions, limestone concrete

16 AVAILABILITY STATEMENT
Unlimited

17 SECURITY CLASSIFICATION (This report)
Unclassified

18 NUMBER OF PAGES
70

19 SECURITY CLASSIFICATION (This page)
Unclassified

20 PRICE
$

☆U.S. GOVERNMENT PRINTING OFFICE: 1984—776-027 / 4274